

Structural Complexity of a Composite Amyloid Fibril

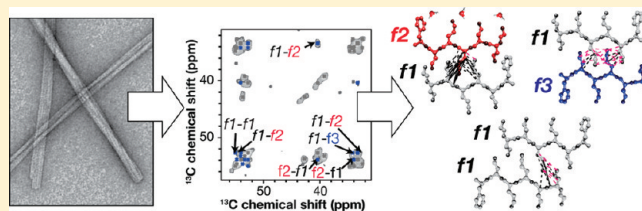
Józef R. Lewandowski,^{ll,†,§} Patrick C. A. van der Wel,^{ll,†,⊥} Mike Rigney,[‡] Nikolaus Grigorieff,[‡] and Robert G. Griffin^{*,†}

[†]Francis Bitter Magnet Laboratory and Department of Chemistry, Massachusetts Institute of Technology, Cambridge, Massachusetts 02139, United States

[‡]Howard Hughes Medical Institute, Brandeis University, Waltham, Massachusetts 02454, United States

S Supporting Information

ABSTRACT: The molecular structure of amyloid fibrils and the mechanism of their formation are of substantial medical and biological importance, but present an ongoing experimental and computational challenge. An early high-resolution view of amyloid-like structure was obtained on amyloid-like crystals of a small fragment of the yeast prion protein Sup35p: the peptide GNNQQNY. As GNNQQNY also forms amyloid-like fibrils under similar conditions, it has been theorized that the crystal's structural features are shared by the fibrils. Here we apply magic-angle-spinning (MAS) NMR to examine the structure and dynamics of these fibrils. Previously multiple NMR signals were observed for such samples, seemingly consistent with the presence of polymorphic fibrils. Here we demonstrate that peptides with these three distinct conformations instead assemble together into composite protofilaments. Electron microscopy (EM) of the ribbon-like fibrils indicates that these protofilaments combine in differing ways to form striations of variable widths, presenting another level of structural complexity. Structural and dynamic NMR data reveal the presence of highly restricted side-chain conformations involved in interfaces between differently structured peptides, likely comprising interdigitated steric zippers. We outline molecular interfaces that are consistent with the observed EM and NMR data. The rigid and uniform structure of the GNNQQNY crystals is found to contrast distinctly with the more complex structural and dynamic nature of these “composite” amyloid fibrils. These results provide insight into the fibril–crystal distinction and also indicate a necessary caution with respect to the extrapolation of crystal structures to the study of fibril structure and formation.



INTRODUCTION

The formation of fibrillar aggregates as a result of extensive protein misfolding is the hallmark of a range of human disorders that include Alzheimer's and Parkinson's disease, type-II diabetes, and Creutzfeldt–Jakob disease. Unfortunately, the detailed mechanisms of toxicity as well as the causes and consequences of the fibril formation remain largely unknown (or at least under debate). One essential piece of the puzzle relates to the molecular structure of the fibrils themselves, and the structural features that may reflect shared attributes of amyloid fibril aggregates.

The paucity of high resolution structural data on amyloid fibrils has contributed to substantial interest in the structure of amyloidogenic peptide fragments that have been studied in a crystalline (rather than fibrillar) state.^{1,2} Elongated microcrystals formed by these peptides were reported to have many of the common biochemical amyloid hallmarks. One of the first such peptide fragments to be studied in great detail was the N-terminal fragment GNNQQNY_{7–13} of the yeast prion-protein Sup35p (the residue numbering in the peptide corresponds to residue numbering in the protein). This peptide was found to adopt a dehydrated parallel β -sheet structure in its crystals. The crystals also featured a characteristic dehydrated interface between β -sheets that relied on steric interactions, and was coined a ‘steric zipper’.¹ This feature was proposed as a potentially common feature shared with other amyloid fibrils. Due to the

absence of tractable, well-characterized amyloid structures, this model peptide system subsequently proved to be a popular target for theoretical studies that aim to characterize the mechanism, kinetics and thermodynamics of amyloid fibril formation, as well as its stability and dye binding mechanisms.^{3–21} Many of these simulations employ the structure of the crystalline form of the peptide as a reference point for the amyloid fibril structure, despite recent experimental uncertainty about structural differences or similarities between the crystals and fibrils.^{22,23}

Magic angle spinning (MAS) NMR is one of the few structural methods that allows us to directly address this uncertainty as it permits structural studies of fibrillar^{24,25} as well as crystalline peptides and proteins.^{26–28} We had therefore previously initiated MAS NMR-based structural studies of GNNQQNY as both nanocrystals and amyloid-like fibrils.^{22,29,30}

One central observation made possible by the use of MAS NMR was that the fibrillar samples contained coexisting peptides in three distinct molecular conformations. Such observations could be explained by the presence of multiple fibril polymorphs, where each conformation (as detected by NMR) would correspond to a different macroscopic and structurally distinct fibril.^{31,32} This type of polymorphism, where GNNQQNY would

Received: April 22, 2011

Published: July 18, 2011

seem able to adopt two distinct crystalline forms and as many as three fibrillar forms, is of significant interest. Polymorphic fibril formation has been reported in vitro and in vivo and is thought to correlate for instance to the strain phenomenon in prion diseases and to variable toxicities for different types of amyloid fibrils.³³ However, our observations could also be accounted for by a different molecular explanation: a single GNNQQNY fibril that contained multiple peptides in different conformations. This is a feature that is not uncommon in crystals, where one macroscopic crystal can contain multiple differently structured monomers within the unit cell. This is for instance seen among the crystals formed by the amyloidogenic peptides studied by Eisenberg et al.,² and would be expected to yield multiple NMR signals for a single site.³⁴ In a fibrillar context, a structurally composite structure has recently been suggested for certain A β fibrils.³⁵

Here, we report on MAS and EM studies of GNNQQNY fibrils aimed to unequivocally establish the nature of the different conformers, which are known to reflect distinctly structured monomers.³⁰ First, we extensively modulate the fibril formation conditions and find that the coexisting fibril forms persist independently of the precise fibrillization conditions. Electron micrographs of the same samples are unable to demonstrate the coexistence of three dominant, visually distinct, fibril morphologies. We then probe intermolecular contacts through specific MAS NMR experiments and find unambiguous intermolecular contacts between the different conformers. Other NMR experiments are performed to detect localized dynamics, in particular for the side chains, as this facilitates resolution of surface-exposed versus fibril-core residues. We then interpret these data in terms of a complex fibrillar assembly in which all three peptide conformers combine to form structurally composite protofilaments that laterally associate to form ribbon-like fibrils. Overall, the data highlight a complexity, both structurally and dynamically, that distinguishes the fibrils from their crystalline counterparts.

MATERIALS AND METHODS

Sample Preparation. GNNQQNY crystalline and fibrillar samples were prepared as described previously,²² using peptides prepared by solid phase peptide synthesis (CS Bio Inc., Menlo Park, CA, and New England Peptide, Gardner, MA). Various differently labeled peptides were prepared, including segmentally and specifically labeled versions (as specified below). Appropriately Fmoc- and side-chain-protected ¹³C- and ¹⁵N-labeled amino acids were obtained from Cambridge Isotope Laboratories (Andover, MA). The general protocol for fibril formation involved the rapid dissolution of the lyophilized peptide in water, resulting in an acidic peptide solution (pH 2–3). Resulting peptide aggregates were packed into MAS rotors, hydrated with excess water.

In order to explore the possibility that the fibril conformers reflect different fibril polymorphs, we purposely varied fibrillization conditions in various ways that could favor the formation of one of the observed or even new polymorphic forms. The resulting fibrils, isotopically labeled with [2-¹³C,¹⁵N-G7] and [U-¹⁵N,¹³C-N8] and 20% diluted into unlabeled peptide, were monitored via MAS NMR spectra. The experimental conditions reflect variations on the original preparation method, which involved the dissolution of peptide at room temperature at a concentration of 20–25 mg/mL.²² Several experiments explore the effect of temperature, as this may differently affect the kinetics of formation for different polymorphs.³⁶ When needed, the solvent was preheated to the initial dissolution temperature (room temperature, 39 °C, or 60 °C) prior to its addition to the peptide, followed by rapid dissolution of the peptide (which was found to be aided by the elevated

temperatures). Subsequently, the solution was allowed to fibrillize, either with or without prior filtration. Filtration was either accomplished by centrifugation through 0.2 μ m Nanosep MF or 3 kDa Nanosep cutoff centrifugal filters (Pall, Port Washington, NY). Note that 0.2 μ m filtration was previously used to favor the formation of crystals in the absence of fibrils^{1,22} and that 3 kDa cutoff membranes may remove pre-existing oligomeric seeds of smaller sizes.³⁷ The temperature during fibril formation was kept constant at the dissolution temperature, reduced gradually by permitting a large water bath to spontaneously and slowly cool down to room temperature, or reduced rapidly by transfer of the dissolved samples to a 4 °C refrigerator. As the pH is also known to effect changes in polymorphism,³⁸ we explored a number of different pHs (no higher than pH ~4 due to lack of solubility near neutral pH). As different polymorphs may have different seeding potentials,³⁹ we also examined the effect of repeated seeding, by seeding several rounds with unlabeled peptide, before doing a final seeding with partially labeled peptide. Mild sonication in a sonicator water bath was also done, as this may similarly cause the (ongoing) generation of seeds within the fibrillizing sample.⁴⁰

Electron Microscopy. Samples were adsorbed on 400 mesh carbon-coated copper grids, which were prepared before use by glow discharging for 1 min. Three to four microliters of solution containing the fibrils was applied to the grid for 1 min and blotted dry, and then grids were briefly rinsed in distilled water and blotted before staining with a 2% uranyl acetate solution. Grids were blotted and allowed to air-dry before being inserted into the microscope. TEM images were collected at 80 kV with an FEI Morgagni 268 (Hillsboro, OR), using an AMT 1k \times 1k CCD camera. Image analysis of the fibril striation widths was done with the image processing package Spider⁴¹ by selecting sections of fibrils and calculating one-dimensional (1D) projections along the length of the fibril. This analysis was only applied to flat sections of fibrils (not showing a twist or bend), which is the typical state of the GNNQQNY fibrils. The pixel size for all of the analyzed fibrils was 7.488 Å/pixel; 2302 measurements were made on 11 fibril samples ranging in width from a single striation to ~20 striations. All of the measurements were made with the same step size. The data from all sample fibrils were added using the same weight for each sample resulting in histogram presented in Figure 3, which was then fitted to 3 Gaussians. Thickness of fibrils was evaluated from occasional crossovers of fibrils in the EM micrographs, where the widths of 13 crossovers were measured by counting pixels.

MAS NMR Methods. Most NMR experiments were performed on a home-built spectrometer designed by Dr. David Ruben, operating at a ¹H Larmor frequency $\omega_{H0}/2\pi = 700$ MHz (16.7 T). Selected experiments were performed on a Bruker Avance spectrometer operating at $\omega_{H0}/2\pi = 900$ MHz (21.4 T). Experiments at 700 MHz employed a Varian triple-channel (HCN) 3.2 mm MAS probe with 3.2 mm MAS rotors from Revolution NMR (Fort Collins, CO). Experiments at 900 MHz used 2.5 mm Bruker MAS rotors and a Bruker 2.5 mm MAS triple-channel HCN probe. The fibrillization condition screening measurements employed ¹³C–¹³C 2D experiments with DARR mixing.⁴²

¹⁵N T₁ Relaxation Measurements. In order to provide a qualitative estimate of the local mobility of ¹⁵N sites in GNN-[U-¹³C,¹⁵N-QQ]-Y sample (and especially the glutamines potentially engaged in a steric zipper interaction) we performed site-specific ¹⁵N T₁ relaxation measurements. We have used a pulse sequence analogous to the one detailed in ref 43. The measurements were done at $\omega_{H0}/2\pi = 700$ MHz, $\omega_r/2\pi = 15$ kHz, employing sample cooling with –8 °C cooling gas. More experimental details can be found in the Supporting Information (SI).

Intermolecular Contacts from PAR and PAIN-CP Experiments. In order to probe intermolecular contacts we performed a series of ¹³C–¹³C PAR⁴⁴ and ¹⁵N–¹³C PAIN-CP^{45,46} experiments on fibril samples with various labeling schemes. ¹³C–¹³C PAR and ¹⁵N–¹³C PAIN-CP techniques are based on a third spin assisted recoupling

Table 1. Experimental protocols for fibril formation

fibrillization condition ^a	description of protocol ^c
normal ^b	peptides were dissolved and fibrillized at room temperature or 4 °C, without agitation
a	peptides were fibrillized at 39 °C
b	dissolution in a 60 °C water bath, fibrillization during gradual cooling to room temperature
c	dissolution at 60 °C, followed by rapid cooling to 4 °C
d	dissolution at 60 °C, followed by 0.2 μ filtration and slow cooling to room temperature
e	5× sequential reseeding using 'normal' protocol
f	fibrillization at room temperature, with ongoing sonication in a water bath
g	fibrillization at room temperature and pH = 3.8
h	fibrillization at room temperature and pH = 2.2

^a Alphabetic labels correspond to those used in Figure 1. All preparations used a peptide concentration of 25 mg/mL. Additional details are in the main text. ^b Conditions previously used for preparing GNNQQNY fibrils.²² ^c Unless specified otherwise, the pH of the dissolved peptide samples was pH ~3 due to the presence of TFA counterions with the purified peptide.²²

(TSAR)⁴⁵ mechanism that is well suited for recording long-range contacts in extensively labeled samples.^{44,45,47,48} ¹³C–¹³C PAR spectra and ¹⁵N–¹³C δp₁ PAIN-CP (with both TSAR and CP mechanism active at the same time) spectra were obtained on fibrils prepared from GNNQQNY, GNNQQNY, and a 50%–50% mixture of GNNQQNY and GNNQQNY, where residues in bold are uniformly ¹³C, ¹⁵N-labeled. These experiments used a 10–14 ms mixing time to allow long-distance transfers, at ω_{H0}/2π = 700 and 900 MHz, with detailed experimental settings as specified in Table S1 (see SI).

RESULTS

Fibril Polymorphism. Our earlier MAS NMR results on GNNQQNY fibril samples revealed constituent peptides in three distinct conformations (here referred to as fibril conformer f1, f2, and f3). In order to probe whether this simply reflected fibril polymorphism, we varied the sample preparation according to the conditions listed in Table 1, using specifically labeled [2-¹³C, ¹⁵N-G]-[U-¹³C, ¹⁵N-N]-NQQNY. Unexpectedly, when fibrils are obtained from these protocols, we consistently observe the same sets of cross peaks (Figure 1b,c), which match our previously assigned fibril shifts (Figure 1a). The spectra in Figure 1 clearly demonstrate the reproducibility of the chemical shifts and signal intensities. Although the extensive overlap in the 1D spectra makes a quantitative analysis difficult, we did integrate the resolved signals in the 2D spectra. These intensities showed some variation in the relative ratios, but on average indicated a ratio of ~43(±3)%:32(±1)%:25(±4)% for conformers 1–3 (see Figure S1, SI). These numbers are similar to our initially published ratio of 39%:35%:27% that was based on fewer (but completely independent) samples.²² Note that these experiments are not highly quantitative in nature, since the polarization transfer process is known to be sensitive to various parameters, such as local structure and dynamics. As we examine in more detail below, these parameters may vary between fibril forms and between samples. As such, it remains uncertain how closely these intensity ratios correlate to population differences. In some of the spectra we detect a presence of a few percent fraction of a fourth form that is too scarce to enable reliable spectral assignment.

Electron Microscopy. Transmission electron microscopy was used to study the various samples prepared for MAS NMR screening as discussed above. The results are shown in Figure 2. Analogous to previous observations^{23,49} the data show that GNNQQNY forms ribbon-like fibrils. While there are subtle variations in the appearance of the fibrils, we were unable to

define a systematic variation of the fibrils from sample to sample (consistent with the MAS results above). If the three sets of NMR signals that we have observed would each correlate to a specific fibril polymorph, one might expect to be able to categorize the fibrils into (three) specific structural categories. However, this does not appear to be the case.

The predominant variation is in the width of the fibril, due to the presence of different numbers of lengthwise striations (e.g., Figure 2e). Upon closer inspection, the striations themselves also vary in their width. We performed 1D projections of the observed intensities along the axis of several fibrils, which provide a better measure of the striation widths (Figure 3). These data indicate that the striations have distributions of widths with the most common values of 51 ± 7 Å, 71 ± 11 Å, and 122 ± 12 Å. We also measured the thickness of the fibrils by examination of (rare) crossover points, resulting in an average thickness of 8.8 pixels (~66 Å) with the standard deviation for all measurements of 1.3 pixels (~10 Å) and the standard error of 0.18 pixels (~1.3 Å).

Site-Specific Dynamics. In earlier experiments we observed indications of more prominent dynamics in the fibrillar samples compared to crystalline samples, in particular in the GNNQQNY labeled segment.³⁰ Here, we explicitly probe these dynamics. First, Figure 4 compares the ¹H–¹³C CP signal to experiments where direct ¹³C excitation is performed. In a direct excitation (DE) experiment the optimal rate for repeating an experiment is determined by the time it takes for a carbon magnetization to recover to equilibrium. Rigid sites are expected to have long ¹³C spin–lattice relaxation rates and thus be severely attenuated (or essentially absent) in experiments employing recycle delays that are short compared to the recovery rate. Thus, in the rigid monoclinic GNNQQNY crystals (see Figure S2, SI) and to a lesser extent in the orthorhombic crystals (Figure 4a,b) almost all of the DE NMR signals are strongly attenuated. The strongest signals, with the fastest relaxation and most motion, are seen in the N-terminal glycine. Analogous measurements on the fibrils reveal a rather different picture, indicating a much-increased level of nanosecond dynamics compared to crystals. All three fibril conformers show more pronounced nanosecond motions at the N-terminus, where the Gly ¹³C sites have shorter T₁'s (even compared to the crystals). Remarkably, it is specifically the fibril conformer f2 that exhibits by far the highest amplitude motions, in a highly localized fashion: the side chain of Q11 of this conformer is highly mobile. We also see a smaller but non-negligible amount of nanosecond motion at its nearby Asn side chains (N12 and most likely N9). We remark that under these

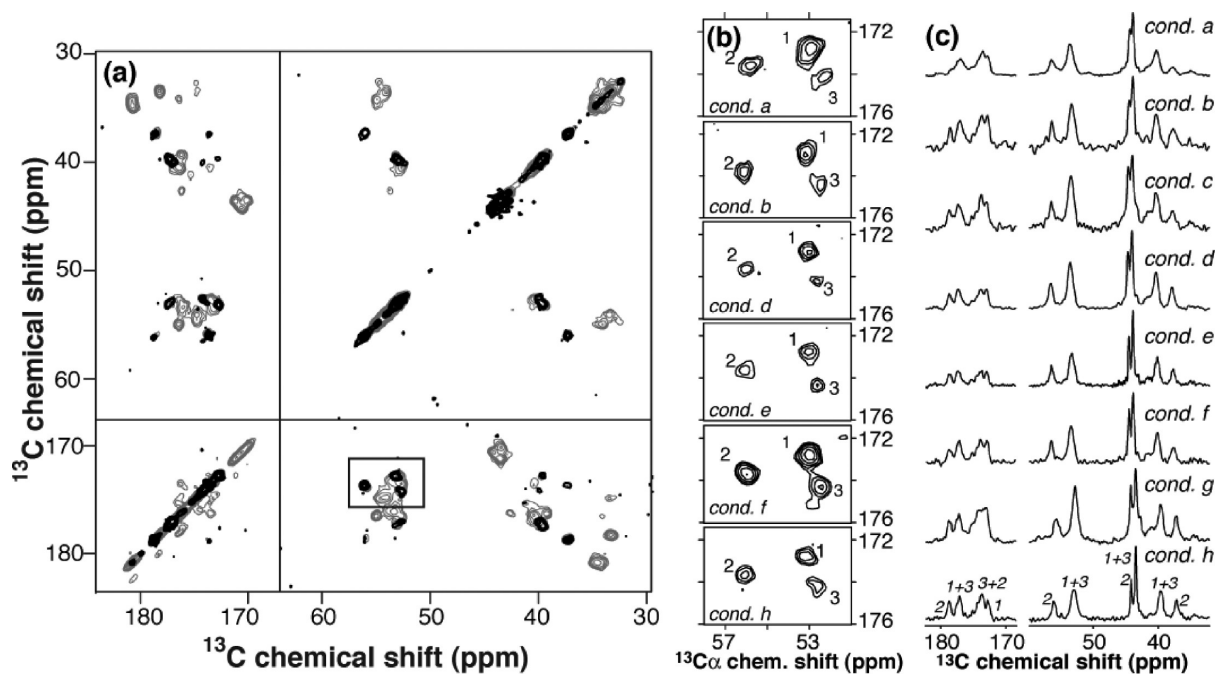


Figure 1. SSNMR screening of $[2\text{-}^{13}\text{C},^{15}\text{N-G}]\text{-}[U\text{-}^{13}\text{C},^{15}\text{N-N}]\text{-NQQNY}$ fibrils prepared under varied conditions. (a) 2D ^{13}C - ^{13}C DARR experiment on $[2\text{-}^{13}\text{C},^{15}\text{N-G}]\text{-}[U\text{-}^{13}\text{C},^{15}\text{N-N}]\text{-NQQNY}$ fibrils (solid black; 100 ms mixing time), comparing these fibrils to previously acquired data on GNNQQNY fibrils (gray background; 12 ms mixing time, bold typeface indicates $[U\text{-}^{13}\text{C},^{15}\text{N}]\text{-}$ labeled residues).²² (b) Highlighted subsections (boxed in (a)) for $[2\text{-}^{13}\text{C},^{15}\text{N-G}]\text{-}[U\text{-}^{13}\text{C},^{15}\text{N-N}]\text{-NQQNY}$ fibrils prepared under a variety of conditions. (c) 1D ^1H - ^{13}C CP spectra, where the previously identified fibril conformers are indicated by the numerals 1–3 (bottom spectrum). All $[2\text{-}^{13}\text{C},^{15}\text{N-G}]\text{-}[U\text{-}^{13}\text{C},^{15}\text{N-N}]\text{-NQQNY}$ fibrils were isotopically dilute. The fibril preparation conditions are indicated in italics, and can be found in Table 1.

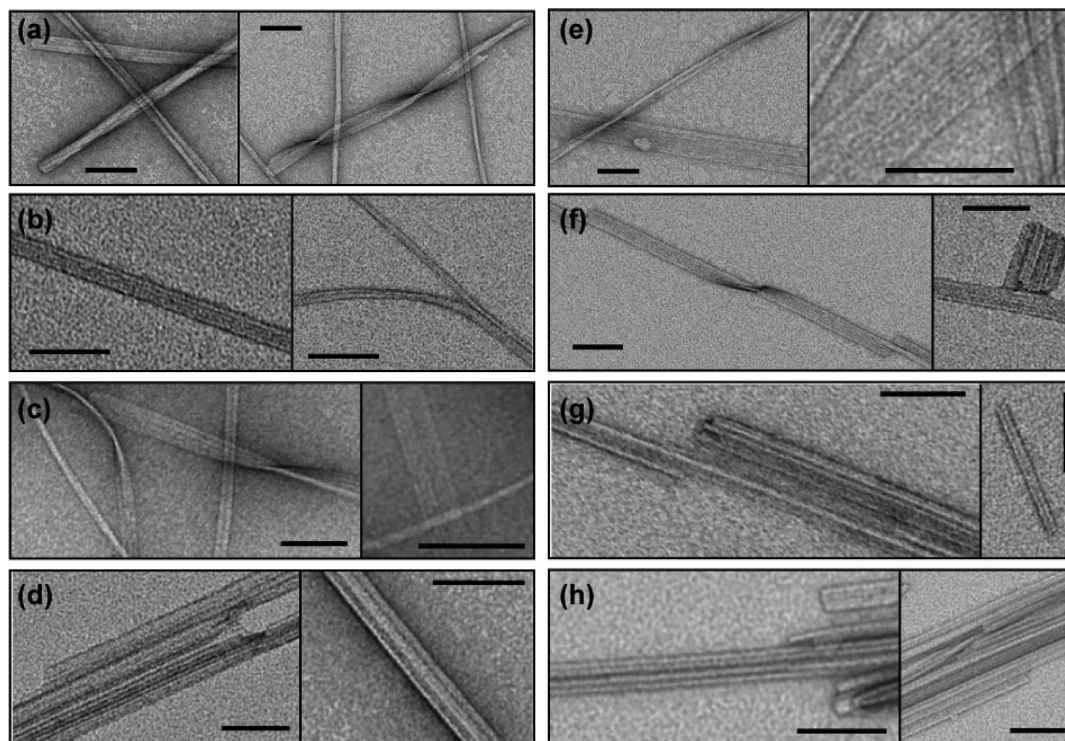


Figure 2. Transmission electron micrographs of negatively stained fibrils of $[2\text{-}^{13}\text{C},^{15}\text{N-G}]\text{-}[U\text{-}^{13}\text{C},^{15}\text{N-N}]\text{-NQQNY}$ prepared under varied conditions. The fibril formation conditions were: (a) at 39 °C, (b) slow cooling from 60 to 20 °C, (c) rapid cooling from 60 to 4 °C, (d) additional 0.2 μ filtration at 60 °C, then slowly cooled, (e) 5 \times reseeded, (f) sonication during fibrillization, (g) fibrillization at pH 2.8, and (h) at pH 3.8. See also Table 1. Black bars in the figures indicate 100 nm scale.

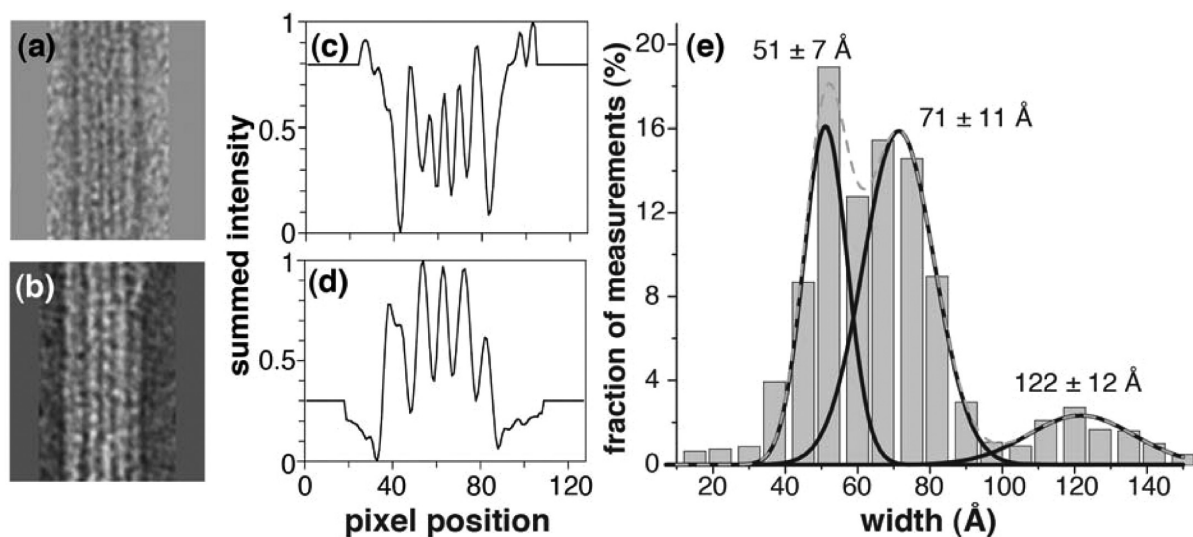


Figure 3. (a,b) Segments featuring straight and flat fibrils were extracted from the TEM data. (c,d) A 1D ('vertical') projection was used to average the pixel intensities (each pixel is 7.488 Å wide). (e) Histogram of trough-to-trough striation widths in GNNQQNY fibrils, which was fitted to 3 Gaussians yielding dominant striation widths of 51 ± 7 Å, 71 ± 11 Å, and 122 ± 12 Å.

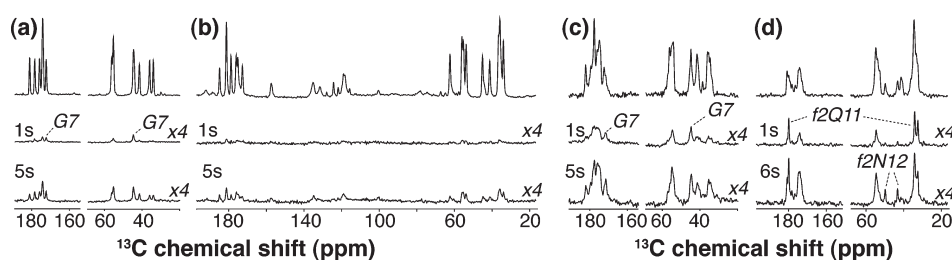


Figure 4. One dimensional ^{13}C ssNMR spectra obtained using $^1\text{H}-^{13}\text{C}$ cross-polarization (top row) or via direct carbon excitation (bottom rows; scaled $\times 4$). Samples: (a) orthorhombic GNNQQNY crystals; (b) orthorhombic GNNQQNY crystals; (c) GNNQQNY fibrils; (d) GNNQQNY fibrils. The middle and bottom rows show direct ^{13}C excitation data with recycle delays of 1 and 5 s, respectively, conditions that favor signals with a short ^{13}C T_1 relaxation time, which can reflect higher than average amplitude nanosecond motions. Panels (a) and (c) show increased nanosecond mobility for the N-terminal Gly in both crystals and fibrils, although the motion is more pronounced in the latter. On the basis of these data the fibrils appear more mobile overall on the nanosecond time scale, but the most striking dynamics are seen in conformer 2. The Q11 side chain of conformer 2 (panel d) is highly dynamic, but higher than average mobility is also seen in its N12 and possibly N9 resonances (panels d and c).

experimental conditions we cannot easily access the site-specific ^{13}C spin–lattice relaxation rates due to the rate averaging by proton-driven spin diffusion (PDSD), which may allow mobile sites to indirectly affect the apparent relaxation rates of nearby (rigid) atoms.⁵⁰ Nonetheless, the employed strategy should yield qualitative and localized information about mobile sites with spin–lattice relaxation rates on the order of, or faster than, the PDSD rates.

Additional evidence for the mobility specific to the side chain of Q11 in fibril f2 was obtained from ^{15}N spin–lattice relaxation rate (R_1) measurements of the GNNQQNY fibrils. The measured R_1 values are plotted in Figure 5b and reported in Table S2 in SI. The majority of the ^{15}N sites (both backbone and side-chain) have R_1 values in the range of 0.04 – 0.09 s^{-1} (typical R_1 's of the backbone nitrogens in secondary structure elements of microcrystalline proteins^{51–54}) indicating that they are rather rigid. The notable exception is the Q11N ϵ site in f2 that, as shown in Figure 5a, relaxes much faster than the corresponding ^{15}N sites in the other two fibril forms (in the same sample). The R_1 of 2.27 s^{-1} indicates a high amplitude nanosecond motion at this site (to put things into perspective: Lipari–Szabo model free

analysis^{55,56} for unrestricted motion in the absence of overall tumbling indicates a minimum T_1 at 700 MHz that corresponds to an R_1 of ~ 2.7 s^{-1}), consistent with the ^{13}C -based data above.

An analogous picture emerges from observation of motionally averaged one-bond CN couplings as determined by TEDOR⁵⁷ experiments on GNNQQNY fibrils. The mixing times at which maximum one-bond polarization transfer is reached for most of the GlnN ϵ -C δ and Asn12N δ -C γ are very similar to the backbone one-bond CN cases and indicate a rather rigid environment (with order parameters $S^2 \sim 0.9$ for motions up to the millisecond time scale). Again the notable exception is f2Q11N ϵ -C δ for which the polarization builds up much more slowly due to the higher amplitude motion (with order parameter $S^2 \sim 0.2$ for motions up to the millisecond time scale) at the site (see Figure S3, SI).

Unambiguous Contacts between Different Conformers.

The lack of sensitivity to the varied preparation conditions appears to support the idea that the multiple fibril conformers are due to a single “composite” protofilament assembly rather than macroscopic fibril polymorphism. Such a model would predict the existence of intimate contacts between the fibril

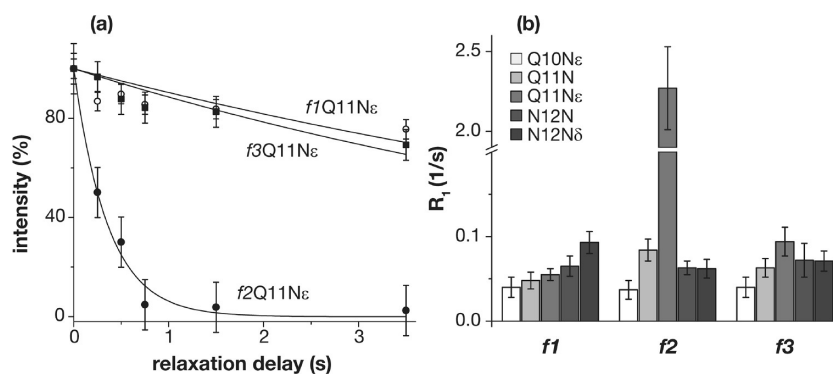


Figure 5. ^{15}N longitudinal relaxation measurements on GNNQQNY fibrils. (a) Q11 side chain nitrogens in all three fibril forms, highlighting the pronounced mobility of the Q11 side chain in f2. (b) Overview of R_1 values for nitrogens Q11N, N12N, Q10N ϵ , Q11N ϵ , and N12N δ in fibril forms 1–3. The Q10N is not listed since it did not generate a cross peak in these NCO 2D experiments (N9C' was not labeled). Note the discontinuous scale on the y-axis.

conformers. In order to look for such contacts, we used two TSAR-based techniques, ^{13}C – ^{13}C PAR⁴⁴ and ^{15}N – ^{13}C PAIN-CP,^{45,46} to probe medium/long distance ^{13}C – ^{13}C and ^{15}N – ^{13}C contacts. These experiments provide an effective means to sample ^{13}C – ^{13}C (PAR) and ^{13}C – ^{15}N (PAIN-CP) distances up to 7 Å and 6 Å, respectively, while limiting the extent of short-distance relayed transfers.^{27,44} The high level of spectral overlap and chemical shift degeneracy of the labeled sites make it often challenging to obtain unambiguous assignments for the observed cross peaks. The level of ambiguity is increased also by the occasional presence of observable peaks due to the fourth fibril form, which constitutes a very small fraction compared to the three dominant fibril forms but may yield short-distance cross peaks that are of comparable intensity to the long distance cross peaks involving other fibril forms.

Figures 6 and 7 show PAR and PAIN-CP spectra employing long mixing times recorded on samples with varying labeling patterns. In these spectra we identified *intermolecular* cross peaks, which are indicated as blue crosses. These cross peaks were identified as unequivocally intermolecular through comparison to simulated spectra of possible intramolecular contacts based on known assignments, peak positions in reference CMRR data⁵⁸ that provide covalent connectivities (see Figure S4, SI), and by considering the sample composition (for details see below). Some of these intermolecular interactions can also be assigned unambiguously, as listed in Table 2. This revealed several cross peaks between *different* fibril conformers, interacting through various side-chain–side-chain interactions. Such data demonstrate that these conformers must be in close contact within the fibrils and thus conclusively support the idea that the GNNQQNY fibrils have an inherently composite structure within the protofilaments.

Identification of Intermolecular Interfaces. To define the interactions that make up these intermolecular interfaces between the conformers it is necessary to also consider the more ambiguous intermolecular cross peaks. To determine the most probable and eliminate the most unlikely assignments while at the same time exploring the nature of the intersheet interactions, we relied on an approach analogous to the network anchoring concept, i.e. that the correct assignment has to produce a self-consistent network of contacts.⁵⁹ A more detailed description of the followed protocol is included in the SI, along with a list of all unambiguously intermolecular cross peaks with the assignments and intermolecular interactions and interfaces that they support

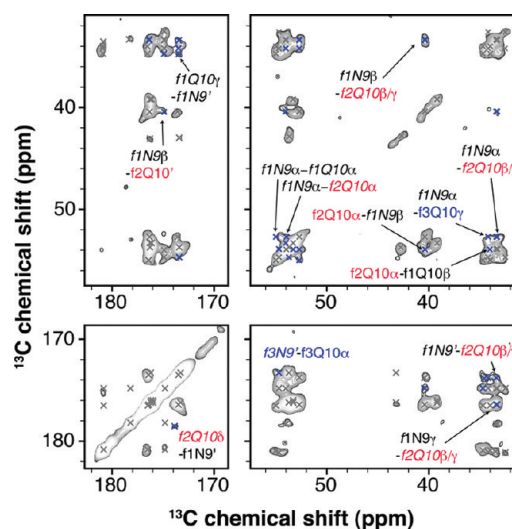


Figure 6. ^{13}C – ^{13}C PAR spectrum on a 50%–50% mixture of GNNQQNY and GNNQQNY fibrils used for anchoring our analysis of intermolecular contacts. The experiment was performed at $\omega_{\text{OH}}/2\pi = 700$ MHz and $\omega_r/2\pi = 10$ kHz and employed 14 ms PAR mixing. Gray crosses indicate cross peaks that can be explained with intramolecular contacts. Unambiguously intermolecular cross peaks are indicated with blue crosses. Unambiguous assignments are indicated in italics. Ambiguous assignments consistent with the proposed side-chain–side-chain interfaces are denoted using regular font. The assignments are color coded as: f1: black, f2: red, and f3: blue.

(Table S3, SI). This analysis resulted in proposed quaternary structural models that are most consistent with these constraints. To facilitate the discussion of these models we refer to the sheet–sheet interactions as involving either the ‘odd face’ (OF) or ‘even face’ (EF) of each conformer, since β -strands present their odd- and even-numbered side chains to opposite sides. When two parallel, in-register β -sheets come together to form an intersheet interface, the peptides in the two sheets can either be aligned (in terms of their N-to-C direction), or go in opposite directions. When the β -sheets are aligned in this context, we refer to the corresponding interface as a parallel, and otherwise as an antiparallel interface. In both known crystalline GNNQQNY assemblies the steric zipper is formed by the EFs from two parallel β -sheets in an antiparallel fashion (*apEF-EF*), the

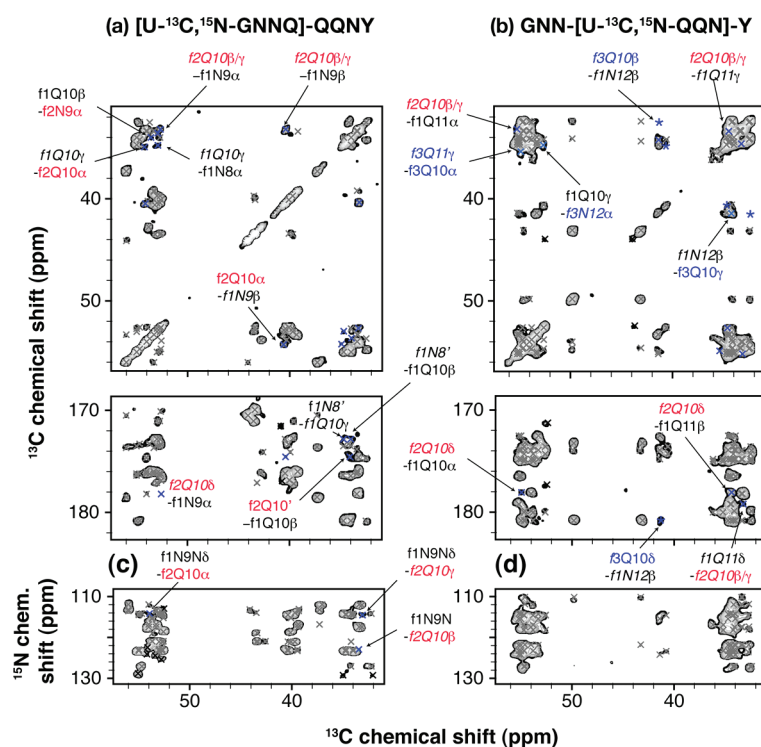


Figure 7. PAR and PAIN-CP spectra on (a,c) GNNQQNY and (b,d) GNNQQNY fibrils with highlighted unambiguously intermolecular cross peaks. Experimental conditions: (a) 10 ms ^{13}C - ^{13}C PAR mixing at $\omega_r/2\pi = 20$ kHz. (b) 10 ms ^{13}C - ^{13}C PAR, $\omega_r/2\pi = 11.3$ kHz. (c) 10 ms δp_1 PAIN-CP mixing, $\omega_r/2\pi = 14.1$ kHz. (d) 14 ms δp_1 PAIN-CP, $\omega_r/2\pi = 9.5$ kHz. Crosses and labeling are as in Figure 6 (unambiguously intermolecular cross peaks are indicated with blue crosses). In addition, the cross peaks from the minor fourth fibril form are indicated with black crosses. Blue stars (b) indicate positions of intermolecular cross peaks that appear in spectra with shorter mixing times (see Figure S4, SI). (b–d) were acquired at $\omega_{\text{H}_0}/2\pi = 700$ MHz and (a) at 900 MHz.

Table 2. List of Unambiguous Intermolecular Cross Peaks in PAR and PAIN-CP Spectra^a

	assignment	spectrum ^b	classification ^c
backbone – backbone	f1N9C α -f1Q10C α	PAR on Q/N mix	f1BB-f1BB
	f2N9C α -f2Q10C α	PAR on Q/N mix	f2BB-f2BB
	f3N9C α -f3Q10C α	PAR on Q/N mix	f3BB-f3BB
	f3N9C' α -f3Q10C α	PAR on Q/N mix	f3BB-f3BB
	f1N9C α -f2Q10C α	PAR on Q/N mix	f1BB-f2BB
backbone – side chain	f1N9C'-f1Q10C γ	PAR on Q/N mix	f1BB-f1EF
	f1N8C'-f1Q10C γ	PAR on GNNQ	f1BB-f1EF
	f1N9C α -f2Q10C $\beta/C\gamma$	PAR on Q/N mix	f1BB-f2EF
	f1N9C'-f2Q10C $\beta/C\gamma$	PAR on Q/N mix	f1BB-f2EF
	f2Q10C δ -f1N9C'	PAR on Q/N mix	f2EF-f1BB
	f1N9C β -f2Q10C $\beta/C\gamma$	PAR on Q/N mix	f1OF-f2EF
side chain – side chain	f1Q11C δ -f2Q10C γ	PAR on QQN	f1OF-f2EF
	f1N9C β -f2Q10C $\beta/C\gamma$	PAR on GNNQ	f1OF-f2EF
	f3Q10C β -f1N12C β	short PAR on QQN	f3EF-f1EF

^a These are all are both unambiguously intermolecular and unambiguously fully assigned (with a chemical shift tolerance of ± 0.3 ppm). ^b Sample composition in shorthand: “Q/N mix”: 50%–50% mixture of GNNQQNY and GNNQQNY; “GNNQ”: GNNQQNY; “QQN”: GNNQQNY. ^c Observed contacts classified as backbone (BB) or side-chain contacts on the even-residue face (EF) or odd-numbered residue face (OF) of the peptides. Listed intraform contacts are necessarily intermolecular by virtue of the applied labeling schemes.

so-called ‘dry interface’, whereas the antiparallel OFs (*apOF-OF*) constitute the ‘wet interface’.²

By combining the information from all the spectra we are able to propose a number of intermolecular side-chain-to-side-chain interfaces present in the GNNQQNY fibrils. Next, we will discuss the various data that support specific proposed interfaces.

The observed contacts supporting each interface can be categorized into completely unambiguously assigned intermolecular cross peaks, intermolecular cross peaks with a majority of ambiguous assignments consistent with the proposed interface, and ambiguous contacts that support the proposed interface but that could also be explained by an intramolecular assignment.

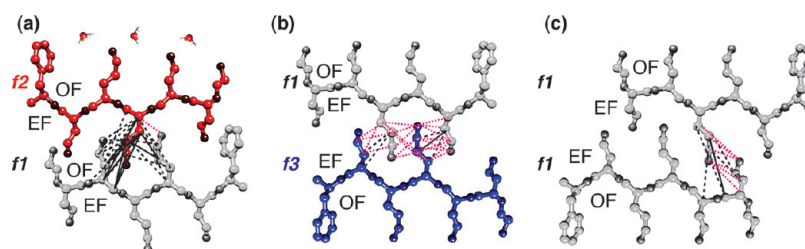


Figure 8. Schematic illustrations of the intersheet interfaces consistent with the long-mixing PAR and PAIN-CP data. Solid lines indicate unambiguously intermolecular and unambiguously assigned cross peaks supporting the given interface. Dashed black lines indicate unambiguously intermolecular and partially or fully ambiguously assigned cross peaks based on the proposed interface. Dashed magenta lines indicate that predicted peaks are present in the spectra but cannot be unambiguously identified as intermolecular (i.e., there is a plausible intramolecular assignment within the chemical shift tolerance). OF and EF define odd and even faces of the β -strands. Note that the torsion angles are only schematic (i.e., arbitrarily generated in Chimera) and do not reflect the real conformation. Although (a) is shown as an antiparallel interface, we cannot exclude a parallel interface due to limitations in the available labeling patterns (see text). The apparent symmetry of the resonances of peptides in the 1–1 interface suggests an antiparallel zipper.³⁴ Water molecules are drawn in (a) to indicate solvent-exposed face.

The proposed interfaces are schematically illustrated in Figure 8, which includes a graphical indication of the supporting contacts that were experimentally observed.

1. Interactions between Conformers 1 and 2. The PAR spectrum of the 50%/50% GNNQQNY/GNNQQNY mixture (Figure 6) proved a useful starting point for assigning the intermolecular interfaces, since any observed Q–N or interform N–N or Q–Q cross peaks (i.e., cross peaks arising from contacts between different conformers) are necessarily intermolecular. This allows identification of intermolecular cross peaks that in GNNQQNY samples would overlap with likely intramolecular assignments. Moreover, since only a single Asn is labeled (N9) this spectrum helps us to avoid some of the assignment ambiguities present in other spectra (between N8 and N9). For the identification of the sheet–sheet interfaces (analogous to the steric zipper motif), we first focus on the side-chain to side-chain contacts. For example, in this PAR spectrum, cross peaks between side chains of f2Q10 and f1N9 indicate the presence of a *f1OF-f2EF* sheet–sheet interface. Intermolecular cross peaks involving backbone sites are generally less informative about sheet–sheet interfaces (due to the large backbone-to-backbone distance between sheets in typical amyloid structure), but they do provide other useful information. The occurrence of intermolecular, but intraform, N9C α -Q10C α cross peaks for all conformers is consistent with each of the fibril forms forming in-register parallel β -sheets.³⁰ Furthermore, lack of other backbone-to-backbone interform cross peaks (except for f2Q10C α -f1N9C α , which is consistent with the f1-f2 contacts that characterize the observed *f1OF-f2EF* interactions between β -sheets), excludes the presence of parallel β -sheets containing multiple conformers within each sheet.

Complementing the data above, the ¹³C–¹³C PAR and ¹⁵N–¹³C PAIN-CP data on differently labeled samples (see Figure 7) help to resolve specific uncertainties and support the consistency-checking phase of the data analysis. For instance, where limited S/N prevents us from reliable determination of Q–Q side-chain to side-chain contacts in the PAR spectrum above (Figure 6), we obtained better data in spectra on unmixed GNNQQNY and GNNQQNY. These spectra provide additional evidence for an *f1OF-f2EF* interface in the form of f2Q10-f1N9 and f2Q10-f1Q11 cross peaks. With the currently available labeling schemes the observable cross peaks are unable to unambiguously define whether the f1OF-f2EF interface is parallel or antiparallel. One needs contacts between multiple residues

across the interface, to clearly detail the relative orientations of the peptides in the two sheets, but in our peptides only a subset of the residues is labeled, which limits the detectable contacts. In the case of a parallel *f1OF-f2EF* one may expect to observe f2N8-f1G7 and f2N8-f1N9 contacts (in the GNNQQNY sample) or f2N12-f1Q11 (in the GNNQQNY sample) contacts, but the vast majority of such cross peaks are not observed (with exception of ambiguous f2N12C β -f1Q11C γ that could also be assigned to intramolecular f2N12C β -f2Q11C γ even though at the limit of detection and chemical shift tolerance).

2. Interactions between Conformers 1 and 3. The sheet–sheet interface between f1 and f3 is defined as an antiparallel *f1EF-f3EF* interaction by the presence of f1N12-f3Q10 and ambiguous but self-consistent f3N12-f1Q10 cross peaks. Note that some of these cross peaks appear already in 2 and 5 ms PAR spectra (e.g., f1N12C β -f3Q10C β is the strongest at 2 ms PAR mixing and very weak at 10 ms mixing; see SI) suggesting that the corresponding distances are short (<3.5 Å) and thus further supporting the presence, in the fibrils, of tightly packed steric zippers between f1 and f3.

3. Intermolecular Intraform Interactions. The above interfaces involved interactions between different conformers. Such interfaces can also occur between multiple monomers that happen to have the same conformation (as is the case in the GNNQQNY crystals, for instance). These same-to-same interactions are harder to identify, but we do see some indications of such interactions: f1Q10-f1N8 cross peaks suggest the existence of an *f1EF-f1EF* sheet–sheet interface. Analogous intramolecular distances in an extended β -sheet conformation would be >6 Å and as such are not expected to be observed. As in the case of *f1-f2* interface, and due to the available labeling patterns, simply relying on observed interpeptide contacts does not permit the unambiguous determination whether the interface is *apf1EF-f1EF* or *pf1EF-f1EF*. However, the peptides obviously display identical chemical shifts (since they reflect the same ‘conformer’, which is defined on that basis), which indicates an inherent symmetry in the interface. This argues for an *apf1EF-f1EF* interface,³⁴ as shown in Figure 8c. Such an interface also corresponds to the steric zipper present in the crystals and is considered more thermodynamically favorable.²⁰

DISCUSSION

Nature of the GNNQQNY Fibril Conformers. One of the most noted features of our earlier results was the identification of

three distinct fibril signals,²² whose structure we subsequently further characterized.³⁰ However, it remained unclear whether these three coexisting structural conformations in the GNNQQNY fibrils reflected the presence of multiple polymorphic fibrils or could (in part) be explained by the presence of differently structured monomers within a single fibril. Amyloid formation tends to show polymorphic behavior that can be quite sensitive to the fibrillization conditions.³¹ For instance Goto and co-workers have described the remarkable transformation of f218 fibrils of β_2 -microglobulin into f210 fibrils that occur as a result of multiple (re)seeding steps.³⁹ In another study, Verel et al. varied the pH to control the formation of different polymorphs of the cc β -p fibrils.⁶⁰ Preparation under agitated and quiescent conditions results in distinct morphologies of A β fibrils.⁶¹ Different temperatures have also been found to yield different fibril polymorphs of certain amyloids, including Sup35p.^{36,62,63} Remarkably, we see little effect of all of these types of modulations on the identity or even the relative ratio of the fibril forms present in the samples. This in itself argues against multiple fibril morphologies, since one would expect their ratios to be more variable with preparation conditions as polymorphs are likely to form by different mechanisms featuring different kinetics. Detailed EM analyses, which did not reveal three distinguishable sets of morphologies, further support this notion. Our results therefore support an alternative model where multiple conformers together contribute to a complex protofilament structure.

Unequivocal support for this comes from our observation of short- to long-distance contacts in our ¹³C–¹³C and ¹³C–¹⁵N TSAR-mediated experiments, which clearly include intermolecular contacts involving different conformers. Such intermolecular contacts would be unlikely to be observable if the different conformers were part of distinct protofilaments. While the distances that can be seen in TSAR-mediated experiments are relatively long for typical ssNMR measurements,^{44,45,47,48} they are still expected to be less than 6–7 Å for mixing times up to 20 ms. Also, due to the TSAR mechanism we are unlikely to observe extensive relayed transfer, in contrast to, for example DARR experiments.^{27,44} The observed distances then require a very intimate contact between peptides and would be unlikely to occur between different fibrils or even protofilaments. Even the 7 Å-wide ‘wet interface’ within the monoclinic GNNQQNY crystals would be too wide for ¹³C–¹³C or ¹⁵N–¹³C contacts to be seen.²⁹ As such, the observed interform cross peaks necessitate the coexistence of the different conformers within a single protofilament. Note that, unlike the GNNQQNY crystals, it is not uncommon to see multiple nonidentical structures in the unit cell of crystalline polypeptides or proteins, including various of the amyloidogenic peptide crystals reported by Sawaya et al.² (see e.g. PDB entries 2OKZ, 2OMQ, 2OMP, 2ON9, and 2ONA). The highly uniform nature of the GNNQQNY crystals is thus not a general characteristic of these amyloid-like peptide crystals, and thus it is perhaps not that surprising (in retrospect) to see that also the GNNQQNY fibrils contain multiple tightly interacting conformers. One important distinction is that simple straightforward symmetry correlation in our fibrils cannot account for the relative peak intensities. This is in contrast to the crystalline case, where very characteristic intensity ratios may be expected (as discussed by Nielsen et al.³⁴).

Dynamics and Solvent Exposure. In addition to the intermolecular polarization transfer, we also determined localized (side-chain) dynamics. One significant distinguishing feature for

the fibrils compared to the crystals is that we observe drastically increased dynamics in the fibrils. The crystals are relatively ‘dry’ and rigid three-dimensional (3D) structures, which feature only limited motion in a few sites.^{1,2,64} This rigidity is correlated to the strong intrasheet hydrogen bonding and intersheet steric zippering of the structure into a highly stable structure. This is for instance apparent in the X-ray crystallographic temperature factors (Figure S5, SI), which reveal little motion in the monoclinic crystals in particular, aside from its very termini. On the other hand, due to the lack of stabilizing π – π stacking interactions in the orthorhombic crystals we see increased motion in those crystals (as predicted by our NMR data²²). However, this motion is still restricted to sites far from the steric zipper and is limited in magnitude (Figure 4).

In contrast, we report high amplitude nanosecond motions for specific sites in the fibrils, especially in the Q11 side chain of conformer f2. Most residues in the fibrillar peptides, including parts of f2 close to the mobile Gln, remain highly immobilized and β -sheet in structure. Note that the ¹⁵N R_1 values for the other Gln side-chains have values typical of backbone nitrogens (<0.1 s^{–1}) rather than solvent exposed side-chain nitrogens in microcrystalline proteins (usually on the order 0.5–2 s^{–1}).⁶⁵ This implies that all the glutamine side-chains except f2Q11 are sterically restricted and are possibly involved in a highly stabilized steric zipper type of interaction. In contrast, the f2Q11 side chain behaves as if it is fully exposed to the solvent and highly mobile and not involved in stabilizing interactions with other peptides. It is worth noting that the Q11 residues in the crystals are much more restricted (and extensively hydrogen bonded), despite facing the water-pocket present in the wet interface of the monoclinic crystals. All this indicates a surface-exposed location for f2Q11 and thus the conformer 2. This is also consistent with the lack of intermolecular interactions for the f2OF.

Intermolecular Interfaces. We can employ both the dynamics and intermolecular contact information to examine some of the intermolecular interactions that underlie the fibril assembly. It appears that the conformer f2 is exclusively present on the surface of the protofilament as it is the only form that contains side-chains (on its OF) that can move about not hindered by steric interactions. The rigidity of all the Q and N side chains in both f1 and f3 suggests that these conformers are present in the ‘core’ of the fibril. It is tempting to ascribe the rigidity of Gln side chains to their involvement in steric zipper-like interfaces.

We indeed identified interactions consistent with steric zipper interfaces based on the polarization exchange experiments (Figure 8). It seems that f1 is in a direct contact with the buried side of the surface exposed conformer f2 through f1OF–f2EF side-chain–side-chain interfaces. The other face of f1 (f1EF) seems to be in contact with the f3EF as well as with itself. The only remaining face that is unaccounted for because it did not yield unambiguously intermolecular cross peaks with other faces is the f3OF (with f3Q11C γ –f3Q10C α as the only potential candidate for an intermolecular cross peak). Since on the basis of the dynamics data we know that f3OF is most likely in the fibril interior, one possibility would be that f3OF is in a steric zipper interaction with itself. A symmetric antiparallel f3OF–f3OF interface could explain f3Q11C γ –f3Q10C α as an intermolecular contact, while it would not be expected to give many other distinctive intermolecular contacts given our current labeling schemes.

Our data suggest that f1EF is involved in interfaces with both f1EF (i.e., another peptide having the same chemical shifts) and with f3EF, which has differing chemical shifts. More specifically,

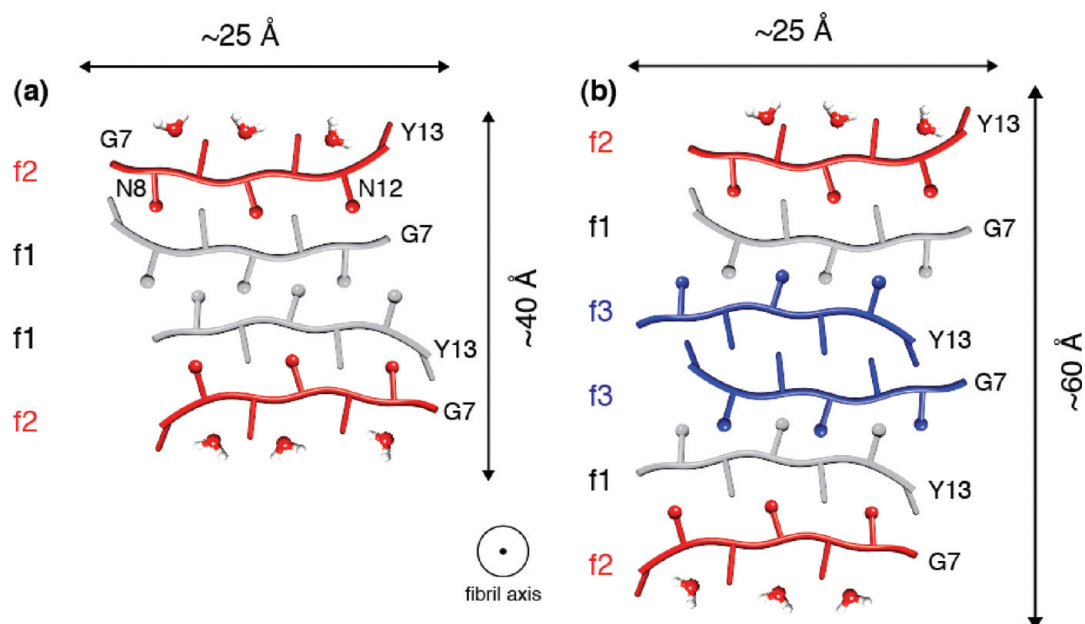


Figure 9. Set of smallest building blocks of the protofilament with side-chain-to-side-chain interfaces consistent with the patterns of our intermolecular cross peaks. The side chains of the even interface (EF) are indicated with balls. The distinct conformations combined with differing intermolecular contributions result in different sets of chemical shifts corresponding to three different forms: f1 is indicated in gray, f2 in red, and f3 in blue. Assembly into protofilaments could involve an association of building blocks through the N- and C-termini (G/Y interface).

f1EF's Q10 interacts with f3 residues N12 and Q10, while its identifiable contacts with another f1 conformer involve residue 8 (compare b and c of Figure 8). This leads us to believe that these contacts must reflect interfaces with two different registries. Although surprising, a promiscuous interface formation by conformer 1 may help explain how it has a significantly higher intensity than the other conformers (and thus may represent the largest population of monomers). The fact that this promiscuity does not result in the chemical shifts for the f1EF side chains showing up as split into two distinct sets of shifts necessitates that the two interfaces must be very similar. Indeed, in both variants of the interface the Q10s are flanked by Gln and Asn, and the only difference is that the terminal Asn's are either flanked by two Asn's or just one Asn. Such a shift in registry without change of the conformation would result in chemical shift changes of less than 0.1 ppm as estimated in SPARTA.⁶⁶

Fibril Assembly. By EM we have observed variability both in the manner in which the protofilaments assemble into ribbon-like fibrils and in the width of individual protofilaments. Despite this morphological variability we observe only three significant conformations by NMR, which all interact with each other. Remarkably, this appears to include a promiscuous intermolecular interface for the most populous conformer f1. We interpret these observations to imply that the protofilament structure must reflect the assembly of similarly structured “composite” building blocks. While different assembly patterns result in “macroscopic” differences in e.g. the striation widths as visible by EM, the “microscopic” (molecular) structure within these basic units appears to be largely invariant (as reflected by the reproduced NMR signals).

Despite having a somewhat underdetermined data set, especially considering the surprising complexities of the GNNQQNY fibril assembly, we can examine some of the features of the underlying protofilament structure. The EM results provided an estimate for the fibril thickness ($66 \pm 10 \text{ \AA}$), as well as striation

widths of $51 \pm 7 \text{ \AA}$, $71 \pm 11 \text{ \AA}$, and $122 \pm 12 \text{ \AA}$. Together, these data delineate the dimensions of the protofilaments that must be composites of the different fibril conformers. We also know that these peptides appear to be present in parallel, in-register β -sheets, adopting an extended backbone conformation,³⁰ with an approximate length of $\sim 25 \text{ \AA}$, and are expected to have a sheet-to-sheet lateral repeat distance of $\sim 10 \text{ \AA}$.⁶⁴

The protofilament dimensions discussed are also consistent with anywhere between 12 and 30 peptides per 4.8 \AA repeat. Considering the interfaces and number of constituent conformers, these dimensions could be explained by combining building blocks containing at most 6 laterally packed β -sheets each. Multiples of such basic building blocks could then associate to generate protofilaments of different widths.

Figure 9 shows potential building block assemblies that are seemingly consistent with our data (note that we lack sufficient data to determine the precise nature of the side-chain–side-chain interface f1–f2, which is shown here as antiparallel). Conformer f2 is the only major surface-exposed conformer, and f1 and f3 must be buried in the fibril interior. This suggests that the smallest possible building block may require *at least* 4 peptides per 4.8 \AA repeat along the fibril axis. Given the presence of cross peaks consistent with f1EF–f3EF, one needs to consider also larger units consisting of at least six peptides per β -sheet layer, where f2 makes up the surface and f1 and f3 together form a dehydrated core. In terms of their approximate dimensions, one would anticipate the 4-mer (e.g., consisting of two f1 and two f2 monomers, see Figure 9a) to have a $\sim 25 \text{ \AA} \times \sim 40 \text{ \AA}$ cross section (perpendicular to the fibril axis) while the 6-mer (Figure 9b) would have cross section closer to $\sim 25 \text{ \AA} \times \sim 60 \text{ \AA}$. Thus 2, 3, or 5 of these building blocks could combine to generate protofilaments of the appropriate dimensions as based on the TEM data. Interestingly, the absence of 100 \AA peak in the histogram of striation widths suggests that combination of 4 such building blocks is not a very likely make of a protofilament. An obvious

explanation for this observation appears to be beyond the currently available data.

Preliminary STEM data performed on fibrils with a majority of 70 Å wide striations (that would consist of 3 building blocks) suggest ~14–16 peptides per 4.8 Å repeat along the length of the fibrils (see SI).

Unfortunately, the variability of the striation width, uncertainties in the precise numbers of peptides in the protofilament (either based on the NMR intensities or by STEM), and the limited number and ambiguity of the intermolecular contacts make an unambiguous detailed reconstruction of the fibril assembly difficult. One possible arrangement would have the building blocks associating via a glycine/tyrosine interface (i.e., their N- and C-termini) to form assemblies of varying width, which would be a multiple of ~25 Å. For instance, one can generate a ~75 Å wide protofilament with 16 peptides per 4.8 Å repeat along the length of the fibril by combining two 6-mer units (Figure 9b) with one of the 4-mer units (Figure 9a). A β -sheet layer of such a protofilament would contain 6 peptides of f1, 6 peptides of f2 and 4 peptides of f3, which would result in f1:f2:f3 relative intensity ratio of 37.5%:37.5%:25%. A ~50 Å protofilament could be constructed from a 6-mer and a 4-mer, resulting in relative intensity ratio of 40%:40%:20%. Finally, ~125 Å protofilaments could be constructed from a combination of ~50 Å and ~75 Å units resulting in a relative intensity ratio of 38.5%:38.5%:23%. These ratios are very close to the average MAS NMR intensity ratios (~43(\pm 3)%:32(\pm 1)%:25(\pm 4)%), although it does not preserve the noted intensity differences between the two most common conformers. A possible contribution could be the increased mobility of f2 sites that could reduce signal intensities in CP-based spectra. An additional effect may be that due to interactions between the building blocks or protofilaments a subpopulation of the normally surface exposed conformer (f2) adopts a different structure when involved in protofilament contacts (i.e., the fibrillar analogue to crystal contacts). This could for instance explain the weak presence of a fourth conformer that may be present at varying intensities (although this is hard to determine quantitatively due to its consistently low intensity). This would also diminish the apparent population of the f2 conformers relative to the number of 'core' monomers and would actually permit one to virtually reproduce the experimental intensity ratios.

Crystals vs Fibrils. The MAS NMR data presented here and elsewhere^{22,30} on the GNNQQNY fibrils provide valuable experimental information on the fibril form of this model peptide. This is of particular interest since the structures of the microcrystals have inspired numerous theoretical analyses aimed at examining various features of amyloid fibrils^{3–19} On the one hand our data indicate certain features in common between the fibrils and crystals, such as a parallel sheet structure³⁰ and the likely presence of (steric) zipper-like interfaces. However, it is also clear that the structural features of the amyloid fibrils are substantially more complex than what is seen in the crystals. At an early stage the latter were identified as relatively devoid of water^{49,64} and adopting a rather rigid structure, with a single consistently homogeneous composition. The simplicity of the resulting assembly may in part be responsible for its popularity and suitability as a computationally tractable model system. However, we^{22,30} and other groups²³ have shown that the amyloid fibrils are substantially more diverse in their structure and dynamics. These results seem consistent with the observations in other amyloid fibril systems, which regularly display

regions of rigid (and protected) β -sheets along with turns and other domains of much increased mobility.^{67–69} Perhaps the incorporation of mobile regions and non- β segments are directly responsible for guiding the formation of the elongated, but narrow fibrils rather than the small, but inherently 3D crystals? What information do our studies provide regarding the different mechanisms leading to crystals and fibrils?

A key determinant of fibril formation is the initial concentration of peptide solution. Observations from various groups now suggest that GNNQQNY forms stable amyloid fibrils only at high concentrations (>20 mg/mL). Marshall et al. have reported that at lower concentrations (<10 mg/mL) the peptide initially forms fibrils that transform in a span of a few days into orthorhombic crystals.²³ On the other hand, in our experience at >20 mg/mL concentration the peptides form extremely stable amyloid fibrils retaining the same properties (provided the samples remain hydrated) over a period of at least two years. As shown here, this aggregation process is remarkably robust with respect to the experimental conditions. At lower concentrations we observed the formation of crystals rather than fibrils,²² although the transient formation of dilute fibrils cannot be excluded.

The nucleation event and the nature of early oligomers likely direct or at least affect the aggregation pathway and the final aggregated state. Both aspects are of high interest for amyloid studies in general, but particularly difficult to study. Experimental and computational studies of the differential aggregation of GNNQQNY may provide a useful model system to understand these key steps in the aggregation process. At low concentrations the initial nucleation of crystal formation may involve just one or two peptides, leading to a symmetric nucleus that results in a crystal lattice with high symmetry. It seems tempting to speculate that increased concentrations facilitate a different pathway, possibly allowing the nucleation event to involve larger numbers of peptides that can form a nonsymmetric nucleus that then leads to the structurally complex fibrils that we observed. Hopefully, further computational and experimental studies can help to elucidate these important early nucleating processes.

CONCLUSION

The atomic-level information available from GNNQQNY crystal structures stimulated numerous speculations and discussions about the core structure of amyloid fibrils. In particular, it inspired a large number of *in silico* studies aimed at extending our understanding of amyloid fibril structure, stability, and formation. Unfortunately, the precise relationship between the clearly distinct crystalline and fibrillar aggregates has remained uncertain. The comparative studies of both crystalline and fibrillar forms by MAS NMR,^{22,30} EM,^{22,23} and fluorescence and linear dichroism²³ suggested that in spite of many similarities between fibrils and crystals there may also be a number of fundamental differences between those two different types of assemblies. Here we have presented a number of new experimental data that reveal a complex supramolecular structure for the GNNQQNY fibrils, which was unaffected by extensive modulation of the fibrillization protocol. Site-resolved structure and dynamics measurements unequivocally show that the different fibril forms are in intimate contact with each other and assemble through a number of different steric zipper interfaces into composite β -sheet-rich building blocks that make up the protofilaments. Our findings complement other experimental and *in silico* studies and should

be of particular value to inform future extensions of such work. Given their independently known crystal structures, GNNQQNY and other amyloid-like *crystalline* peptides may continue to serve as appropriate and convenient *experimental* amyloid-like test cases for the development and demonstration of MAS NMR and other experimental techniques.

■ ASSOCIATED CONTENT

S Supporting Information. Spectra used for the assignment of GNNQQNY fibrils; additional ^{15}N relaxation measurement data and one-bond TEDOR data indicating differential dynamics. Table of unambiguously assigned intermolecular cross peaks along with the sheet–sheet interfaces that they support. STEM data on GNNQQNY fibrils. Histograms of the striation widths in fibrils. Direct ^{13}C excitation 1D spectra for monoclinic GNNQQNY crystals as a function of recycle delay. This material is available free of charge via the Internet at <http://pubs.acs.org>.

■ AUTHOR INFORMATION

Corresponding Author

rgg@mit.edu

Present Addresses

⁵Present address: Department of Chemistry, University of Warwick, Coventry, CV4 7AL, U.K.

[†]Present Address: Department of Structural Biology, University of Pittsburgh School of Medicine, Pittsburgh, PA 15260.

Author Contributions

^{||}These authors contributed equally.

■ ACKNOWLEDGMENT

We thank Marc Caporini, Marvin Bayro, and Paul Guerry for helpful discussions. Molecular graphics images were produced using the UCSF Chimera package from the Resource for Bio-computing, Visualization, and Informatics at the University of California, San Francisco (supported by NIH P41 RR-01081). This research was supported by the National Institutes of Health through Grants EB-003151 and EB-002026. We thank Joseph Wall and Martha Simon for the preliminary STEM data and Rebecca Nelson and David Eisenberg for helpful feedback and suggestions regarding GNNQQNY sample preparation conditions.

■ REFERENCES

- (1) Nelson, R.; Sawaya, M. R.; Balbirnie, M.; Madsen, A. O.; Riek, C.; Grothe, R.; Eisenberg, D. *Nature* **2005**, *435*, 773–778.
- (2) Sawaya, M. R.; Sambashivan, S.; Nelson, R.; Ivanova, M. I.; Sievers, S. A.; Apostol, M. I.; Thompson, M. J.; Balbirnie, M.; Wiltzius, J. J. W.; McFarlane, H. T.; Madsen, A. O.; Riek, C.; Eisenberg, D. *Nature* **2007**, *447*, 453–457.
- (3) Gsponer, J.; Habertühr, U.; Cafilisch, A. *Proc. Natl. Acad. Sci. U.S.A.* **2003**, *100*, 5154–5159.
- (4) Cecchini, M.; Rao, F.; Seeber, M.; Cafilisch, A. *J. Chem. Phys.* **2004**, *121*, 10748–10756.
- (5) Lipfert, J.; Franklin, J.; Wu, F.; Doniach, S. *J. Mol. Biol.* **2005**, *349*, 648–658.
- (6) Zheng, J.; Ma, B.; Tsai, C.-J.; Nussinov, R. *Biophys. J.* **2006**, *91*, 824–833.
- (7) Esposito, L.; Pedone, C.; Vitagliano, L. *Proc. Natl. Acad. Sci. U.S.A.* **2006**, *103*, 11533–11538.

- (8) Zhang, Z.; Chen, H.; Bai, H.; Lai, L. *Biophys. J.* **2007**, *93*, 1484–1492.
- (9) Wu, C.; Wang, Z.; Lei, H.; Zhang, W.; Duan, Y. *J. Am. Chem. Soc.* **2007**, *129*, 1225–1232.
- (10) Tsemekhman, K.; Goldschmidt, L.; Eisenberg, D.; Baker, D. *Protein Sci.* **2007**, *16*, 761–764.
- (11) Strodel, B.; Whittleston, C. S.; Wales, D. J. *J. Am. Chem. Soc.* **2007**, *129*, 16005–16014.
- (12) Knowles, T. P.; Fitzpatrick, A. W.; Meehan, S.; Mott, H. R.; Vendruscolo, M.; Dobson, C. M.; Welland, M. E. *Science* **2007**, *318*, 1900–1903.
- (13) Meli, M.; Morra, G.; Colombo, G. *Biophys. J.* **2008**, *94*, 4414–4426.
- (14) De Simone, A.; Esposito, L.; Pedone, C.; Vitagliano, L. *Biophys. J.* **2008**, *95*, 1965–1973.
- (15) Wang, J.; Tan, C.; Chen, H.-F.; Luo, R. *Biophys. J.* **2008**, *95*, 5037–5047.
- (16) Esposito, L.; Paladino, A.; Pedone, C.; Vitagliano, L. *Biophys. J.* **2008**, *94*, 4031–4040.
- (17) Vitagliano, L.; Esposito, L.; Pedone, C.; De Simone, A. *Biochem. Biophys. Res. Commun.* **2008**, *377*, 1036–1041.
- (18) Reddy, G.; Straub, J. E.; Thirumalai, D. *Proc. Natl. Acad. Sci. U.S.A.* **2009**, *106*, 11948–11953.
- (19) Periole, X.; Rampioni, A.; Vendruscolo, M.; Mark, A. E. *J. Phys. Chem. B* **2009**, *113*, 1728–1737.
- (20) Park, J.; Kahng, B.; Hwang, W. *PLoS Comput. Biol.* **2009**, *5*, e1000492.
- (21) Berryman, J. T.; Radford, S. E.; Harris, S. A. *Biophys. J.* **2009**, *97*, 1–11.
- (22) Van der Wel, P. C. A.; Lewandowski, J. R.; Griffin, R. G. *J. Am. Chem. Soc.* **2007**, *129*, 5117–5130.
- (23) Marshall, K. E.; Hicks, M. R.; Williams, T. L.; Hoffmann, S. V.; Rodger, A.; Dafforn, T. R.; Serpell, L. C. *Biophys. J.* **2010**, *98*, 330–338.
- (24) Tycko, R. Q. *Rev. Biophys.* **2006**, *39*, 1–55.
- (25) Heise, H. *ChemBioChem* **2008**, *9*, 179–189.
- (26) Rienstra, C. M.; Tucker-Kellogg, L.; Jaronec, C. P.; Hohwy, M.; Reif, B.; McMahon, M. T.; Tidor, B.; Lozano-Perez, T.; Griffin, R. G. *Proc. Natl. Acad. Sci. U.S.A.* **2002**, *99*, 10260–10265.
- (27) Bertini, I.; Bhaumik, A.; De Paepe, G.; Griffin, R. G.; Lelli, M.; Lewandowski, J. R.; Luchinat, C. *J. Am. Chem. Soc.* **2010**, *132*, 1032–1040.
- (28) Castellani, F.; van Rossum, B.; Diehl, A.; Schubert, M.; Rehbein, K.; Oschkinat, H. *Nature* **2002**, *420*, 98–102.
- (29) van der Wel, P. C. A.; Hu, K. N.; Lewandowski, J.; Griffin, R. G. *J. Am. Chem. Soc.* **2006**, *128*, 10840–10846.
- (30) van der Wel, P. C. A.; Lewandowski, J. R.; Griffin, R. G. *Biochemistry* **2010**, *49*, 9457–9469.
- (31) Kodali, R.; Wetzel, R. *Curr. Opin. Struct. Biol.* **2007**, *17*, 48–57.
- (32) Fändrich, M.; Meinhardt, J.; Grigorieff, N. *Prion* **2009**, *3*, 89–93.
- (33) Aguzzi, A.; Heikenwalder, M.; Polymenidou, M. *Nat. Rev. Mol. Cell Biol.* **2007**, *8*, 552–561.
- (34) Nielsen, J. T.; Bjerring, M.; Jeppesen, M. D.; Pedersen, R. O.; Pedersen, J. M.; Hein, Kim L.; Vosegaard, T.; Skrydstrup, T.; Otzen, D. E.; Nielsen, N. C. *Angew. Chem., Int. Ed.* **2009**, *48*, 2118–2121.
- (35) Sachse, C.; Fändrich, M.; Grigorieff, N. *Proc. Natl. Acad. Sci. U. S. A.* **2008**, *105*, 7462–7466.
- (36) Nekooki-Machida, Y.; Kurosawab, M.; Nukina, N.; Ito, K.; Oda, T.; Tanaka, M. *Proc. Natl. Acad. Sci. U.S.A.* **2009**, *106*, 9679–9684.
- (37) Evans, K. C.; Berger, E. P.; Cho, C. G.; Weisgraber, K. H.; Lansbury, P. T. *Proc. Natl. Acad. Sci. U.S.A.* **1995**, *92*, 763–767.
- (38) Gosal, W. S.; Morten, I. J.; Hewitt, E. W.; Smith, D. A.; Thomson, N. H.; Radford, S. E. *J. Mol. Biol.* **2005**, *351*, 850–864.
- (39) Yamaguchi, K.; Takahashi, S.; Kawai, T.; Naiki, H.; Goto, Y. *J. Mol. Biol.* **2005**, *352*, 952–960.
- (40) Jarrett, J. T.; Lansbury, P. T. *Biochemistry* **1992**, *31*, 12345–12352.

- (41) Frank, J.; Radermacher, M.; Penczek, P.; Zhu, J.; Li, Y. H.; Ladjadi, M.; Leith, A. J. *Struct. Biol.* **1996**, *116*, 190–199.
- (42) Takegoshi, K.; Nakamura, S.; Terao, T. *Chem. Phys. Lett.* **2001**, *344*, 631–637.
- (43) Giraud, N.; Böckmann, A.; Lesage, A.; Penin, F.; Blackledge, M.; Emsley, L. J. *Am. Chem. Soc.* **2004**, *126*, 11422–11423.
- (44) De Paëpe, G.; Lewandowski, J. R.; Loquet, A.; Bockmann, A.; Griffin, R. G. *J. Chem. Phys.* **2008**, *129*, 245101.
- (45) Lewandowski, J.; De Paëpe, G.; Griffin, R. G. *J. Am. Chem. Soc.* **2007**, *129*, 728–729.
- (46) De Paëpe, G.; Lewandowski, J. R.; Loquet, A.; Eddy, M. T.; Meggy, S.; Bockmann, A.; Griffin, R. G. *J. Phys. Chem.* **2010**, *134*, 095101.
- (47) Lewandowski, J. R.; De Paëpe, G.; Eddy, M. T.; Griffin, R. G. *J. Am. Chem. Soc.* **2009**, *131*, 5769–5776.
- (48) Lewandowski, J. R.; De Paëpe, G.; Eddy, M. T.; Struppe, J.; Maas, W.; Griffin, R. G. *J. Phys. Chem. B* **2009**, *113*, 9062–9069.
- (49) Diaz-Avalos, R.; Long, C.; Fontano, E.; Balbirnie, M.; Grothe, R.; Eisenberg, D.; Caspar, D. L. D. *J. Mol. Biol.* **2003**, *330*, 1165–1175.
- (50) Lewandowski, J. R.; Sein, J.; Sass, H. J.; Grzesiek, S.; Blackledge, M.; Emsley, L. J. *Am. Chem. Soc.* **2010**, *132*, 8252–8254.
- (51) Giraud, N.; Blackledge, M.; Goldman, M.; Böckmann, A.; Lesage, A.; Penin, F.; Emsley, L. J. *Am. Chem. Soc.* **2005**, *127*, 18190–18201.
- (52) Chevelkov, V.; Diehl, A.; Reif, B. *J. Chem. Phys.* **2008**, *128*, 052316.
- (53) Lewandowski, J. R.; Sein, J.; Blackledge, M.; Emsley, L. J. *Am. Chem. Soc.* **2010**, *132*, 1246–1248.
- (54) Yang, J.; Tasayco, M. L.; Polenova, T. *J. Am. Chem. Soc.* **2009**, *131*, 13690–13702.
- (55) Lipari, G.; Szabo, A. *J. Am. Chem. Soc.* **1982**, *104*, 4546–4559.
- (56) Chevelkov, V.; Zhuravleva, A. V.; Xue, Y.; Reif, B.; Skrynnikov, N. R. *J. Am. Chem. Soc.* **2007**, *129*, 12594–12595.
- (57) Hing, A. W.; Vega, S.; Schaefer, J. J. *Magn. Reson.* **1992**, *96*, 205–209.
- (58) De Paëpe, G.; Lewandowski, J. R.; Griffin, R. G. *J. Chem. Phys.* **2008**, *128*, 124503.
- (59) Herrmann, T.; Guntert, P.; Wuthrich, K. *J. Mol. Biol.* **2002**, *319*, 209–227.
- (60) Verel, R.; Tomka, I. T.; Bertozzi, C.; Cadalbert, R.; Kammerer, R. A.; Steinmetz, M. O.; Meier, B. H. *Angew. Chem., Int. Ed.* **2008**, *47*, 5842–5845.
- (61) Petkova, A. T.; Leapman, R. D.; Guo, Z.; Yau, W.-M.; Mattson, M. P.; Tycko, R. *Science* **2005**, *307*, 262–265.
- (62) Chien, P.; DePace, A. H.; Collins, S. R.; Weissman, J. S. *Nature* **2003**, *424*, 948–951.
- (63) Ohhashi, Y.; Ito, K.; Toyama, B. H.; Weissman, J. S.; Tanaka, M. *Nat. Chem. Biol.* **2010**, *6*, 225–230.
- (64) Balbirnie, M.; Grothe, R.; Eisenberg, D. S. *Proc. Natl. Acad. Sci. U.S.A.* **2001**, *98*, 2375–80.
- (65) For example, side-chain Gln and Asn nitrogens in microcrystalline GB1 at $\omega_{\text{H0}}/2\pi = 700$ MHz and ~ 5 °C have typical rates in the 0.6 – 1.5 s⁻¹ range, with an exception of one side chain that has restricted mobility due to the proximity of an aromatic ring. Lewandowski, J. R. (personal communication).
- (66) Shen, Y.; Bax, A. *J. Biomol. NMR* **2007**, *38*, 289–302.
- (67) Siemer, A. B.; Arnold, A. A.; Ritter, C.; Westfeld, T.; Ernst, M.; Riek, R.; Meier, B. H. *J. Am. Chem. Soc.* **2006**, *128*, 13224–13228.
- (68) Sillen, A.; Wieruszkeski, J. M.; Leroy, A.; Ben Younes, A.; Landrieu, I.; Lippens, G. *J. Am. Chem. Soc.* **2005**, *127*, 10138–10139.
- (69) Heise, H.; Hoyer, W.; Becker, S.; Andronesi, O. C.; Riedel, D.; Baldus, M. *Proc. Natl. Acad. Sci. U.S.A.* **2005**, *102*, 15871–15876.

Supporting Information

for

Structural complexity of a composite amyloid fibril

Józef R. Lewandowski, Patrick C.A. van der Wel, Mike Rigney, Nikolaus Grigorieff,
Robert G. Griffin*

Contents:

Experimental details of PAR and PAINCP experiments	S2
Relative intensities of fibril forms	S3
¹⁵ N relaxation measurements	S4
¹³ C- ¹⁵ N dipolar interactions via TEDOR	S6
Identification of intermolecular contacts	S7
B-factors for monoclinic and orthorhombic crystals	S11
References cited in the SI	S12

Experimental details of PAR and PAINCP experiments

Table S1. Experimental details for long-mixing TSAR-based experiments. These experiments were configured to allow efficient detection of long-distance transfers, between ^{13}C sites or from ^{15}N to ^{13}C .

experiment	labeling	$\omega_{\text{H0}}/2\pi$ (kHz)	$\omega_r/2\pi$ (kHz)	$\omega_{^{13}\text{C}}/2\pi$ (kHz)	$\omega_{^{15}\text{N}}/2\pi$ (kHz)	$\omega_{^1\text{H}}/2\pi$ (kHz)	t_{mix} (ms)	^{13}C offset (ppm)	^{15}N offset (ppm)
PAR	[U- ^{13}C , ^{15}N -GNNQ]-QNY	900	20	55	-	50	10	42, 108 ^b	-
PAIN-CP	[U- ^{13}C , ^{15}N -GNNQ]-QNY	700	14.1	39	25	84	10	42, 175.2 ^b	120
PAR	GNN-[U- ^{13}C , ^{15}N -QQN]-Y	700	11.3	59	-	58	10	100	-
PAIN-CP	GNN-[U- ^{13}C , ^{15}N -QQN]-Y	700	9.5	47 ^a	40	50	14	110	120
PAR	50%/50% GN-[U- ^{13}C , ^{15}N -N]-QQNY/ GNN-[U- ^{13}C , ^{15}N -Q]-QNY	700	10	67	-	64	14	100	-

^a with a small ~ 3 kHz ramp on ^{13}C

^b in cases where the CP was performed at different offsets in different experiments, two values are listed

Relative intensities of fibril forms

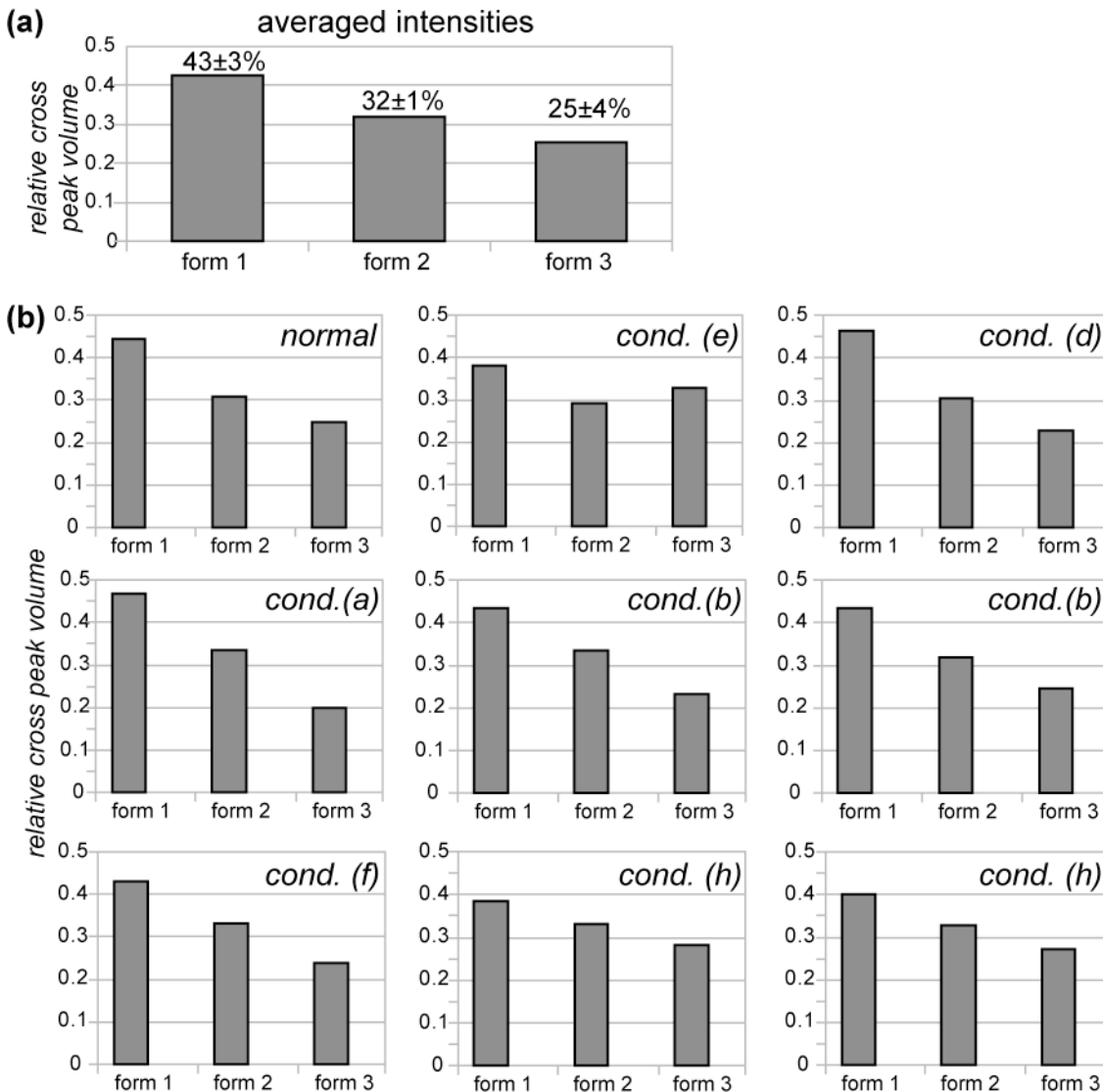


Figure S1. Overview of peak volumes from 2D ^{13}C - ^{13}C spectra, as in Figure 1 in the manuscript. Note that these DARR experiments are not quantitative, due to sensitivities of the magnetization transfer to factors such as structural and motional differences between the different conformers.

¹⁵N relaxation measurements

In order to provide a qualitative estimate of the local mobility in GNN[U-¹³C,¹⁵N-QQN]Y fibrils (and especially the glutamines potentially engaged in a steric zipper interaction) we performed site-specific ¹⁵N T₁ relaxation measurements. These experiments at 700 MHz ($\omega_{H0}/2\pi$) employed a pulse sequence analogous to the one detailed in ref. 1. A series of ¹⁵N-¹³C correlation experiments with ¹⁵N relaxation times of 0, 0.25, 0.5, 0.75, 1.5 and 3.5 s were performed using a 1.5 ms ¹H-¹⁵N CP contact time ($\omega_{1H}/2\pi = 59$ kHz, ¹⁵N ramped through n=-1 Hartmann-Hahn condition, center of the ramp ~ 44 kHz), 4 ms ¹⁵N-¹³C CP contact time ($\omega_{1N}/2\pi = 20$ kHz, ¹³C ramped through n=-1 Hartmann-Hahn condition, center of the ramp ~ 5 kHz, 98 kHz ¹H CW decoupling), and 98 kHz TPPM decoupling during t₁ and t₂ evolution. The R₁ was estimated from the initial slope of relaxation curves² based on the extracted peak intensities (normalized to the intensity of the cross peaks in the spectrum with 0 s relaxation time) fitted to a single exponential function $I = \exp(-R_1 t)$.

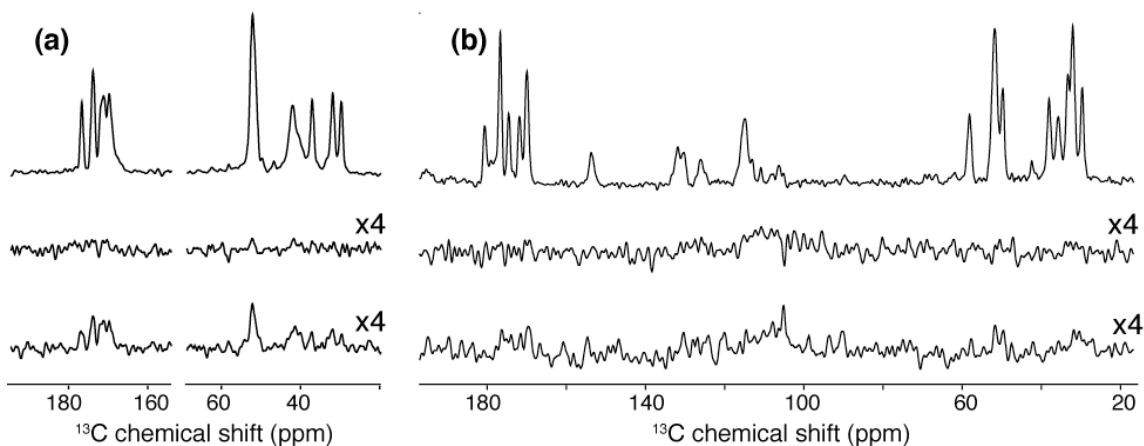


Figure S2. 1D ^{13}C ssNMR spectra employing ^1H - ^{13}C cross polarization (top row) or via direct carbon excitation (bottom rows; scaled x4) of monoclinic GNNQQNY crystals U- ^{13}C , ^{15}N -labeled in residues G7-Q10 (a) or Q10-Y13 (b). The middle and bottom rows show direct ^{13}C excitation data with recycle delays of 1 and 5 s, respectively. The main site featuring faster ^{13}C T_1 relaxation is the N-terminal Gly in (a). These spectra were obtained at $\omega_r/2\pi = 8\text{kHz}$ on a 500MHz spectrometer, using a 4mm Chemagnetics HCN CP-MAS probe.

Table S2. ^{15}N longitudinal relaxation rates obtained on GNN-[U- ^{13}C , ^{15}N -QQN]-Y fibril samples. Experiments were done at $\omega_{\text{H0}}/2\pi = 700\text{ MHz}$ (see text for more details).

	Site	R_1 [1/s]	Standard Error	$T_1(=1/R_1)$ [s]
Fibril 1	Gln ₁₀ N _ε *	0.040	±0.012	24.9
	Gln ₁₁ N	0.048	±0.010	20.8
	Gln ₁₁ N _ε	0.055	±0.007	18.2
	Asn ₁₂ N	0.065	±0.012	15.3
	Asn ₁₂ N _δ	0.093	±0.013	10.7
Fibril 2	Gln ₁₀ N _ε	0.037	±0.011	27.2
	Gln ₁₁ N	0.084	±0.013	11.9
	Gln ₁₁ N _ε	2.27	±0.262	0.4
	Asn ₁₂ N	0.063	±0.008	16.0
	Asn ₁₂ N _δ	0.062	±0.011	16.1
Fibril 3	Gln ₁₀ N _ε *	0.040	±0.012	24.9
	Gln ₁₁ N	0.063	±0.011	15.8
	Gln ₁₁ N _ε	0.094	±0.017	10.6
	Asn ₁₂ N	0.072	±0.020	13.9
	Asn ₁₂ N _δ	0.071	±0.012	14.1

* These sites are not resolved in 2D NCO spectra – the same relaxation rate assumed for both sites.

^{13}C - ^{15}N dipolar interactions via TEDOR

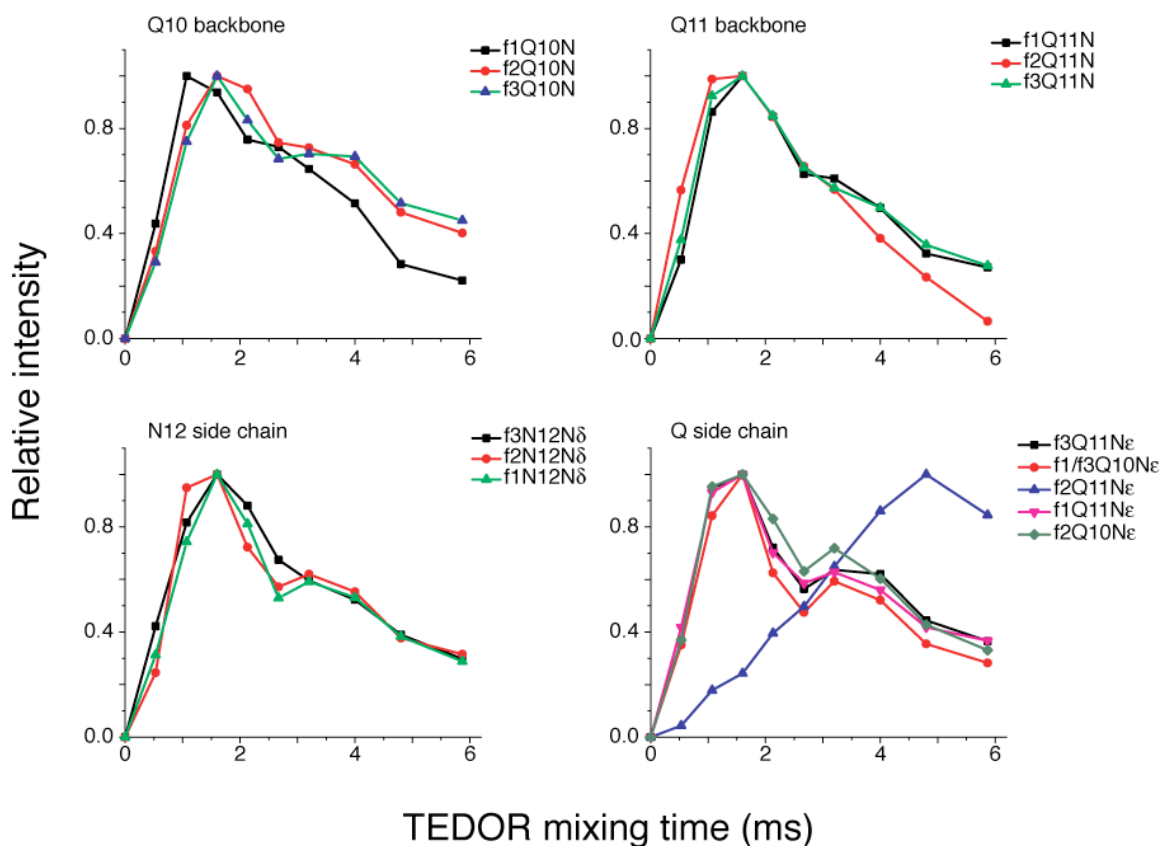


Figure S3. One-bond CN polarization transfer curves as a function of TEDOR mixing time. Note the substantially longer mixing time necessary for the f2Q11Nε-Q11Cγ to reach the maximum cross peak intensity suggesting increased mobility of f2Q11 side chain. The experiments were performed on GNN-[U- ^{13}C , ^{15}N -QQN]-Y sample at $\omega_{\text{OH}}/2\pi = 700$ MHz and $\omega_r/2\pi = 10$ kHz. The intensities are normalized to maximum intensity.

Identification of intermolecular contacts

In the first step, based on the known spectral assignments, we have generated a peak list for all possible *intramolecular* contact combinations that could be visible in the ^{13}C - ^{13}C PAR and PAIN-CP spectra with given mixing times, which were chosen to yield contacts up to $\sim 5\text{-}6$ Å. Since we know that the fibril backbone conformations basically reflect a β -sheet structure, {van der Wel, #218} we employed the monomer conformation from the monoclinic crystal as a framework for evaluating likely intramolecular cross peaks (up to ~ 6 Å). A chemical shift tolerance of ± 0.3 ppm was used and, whenever possible, the peaks were also lined-up visually with known intramolecular peaks elsewhere in the same spectrum (to account for small shifts due to the slightly different experimental conditions, such as differences in spinning rates). Experimentally observed cross peaks that were unaccounted for in this process were then checked for possible inter-form assignments.

These intermolecular cross peaks were then checked for consistency with different side-chain-side-chain interfaces. After verifying all unambiguously *intermolecular* cross peaks we also examined other cross peaks (i.e. those presumed to possibly be intramolecular before) for consistency with candidate interfaces. For example, if we observe an unambiguously intermolecular f3Q10C β -f1N12C β we also checked for occurrence of a cross peak between f1N12C β and f3Q10N ϵ or f3Q10C γ etc. The presence of such cross peaks served as positive ambiguous restraints supporting the interface and absence of cross peaks was used as a negative restraint against the proposed interface. A given side-chain-to-side-chain interface was considered a viable solution if its assumption led to multiple self-confirming assignments. A compiled list of all the unambiguously intermolecular cross peaks along with the assignments and the types of intermolecular interfaces that they support can be found in Table S3.

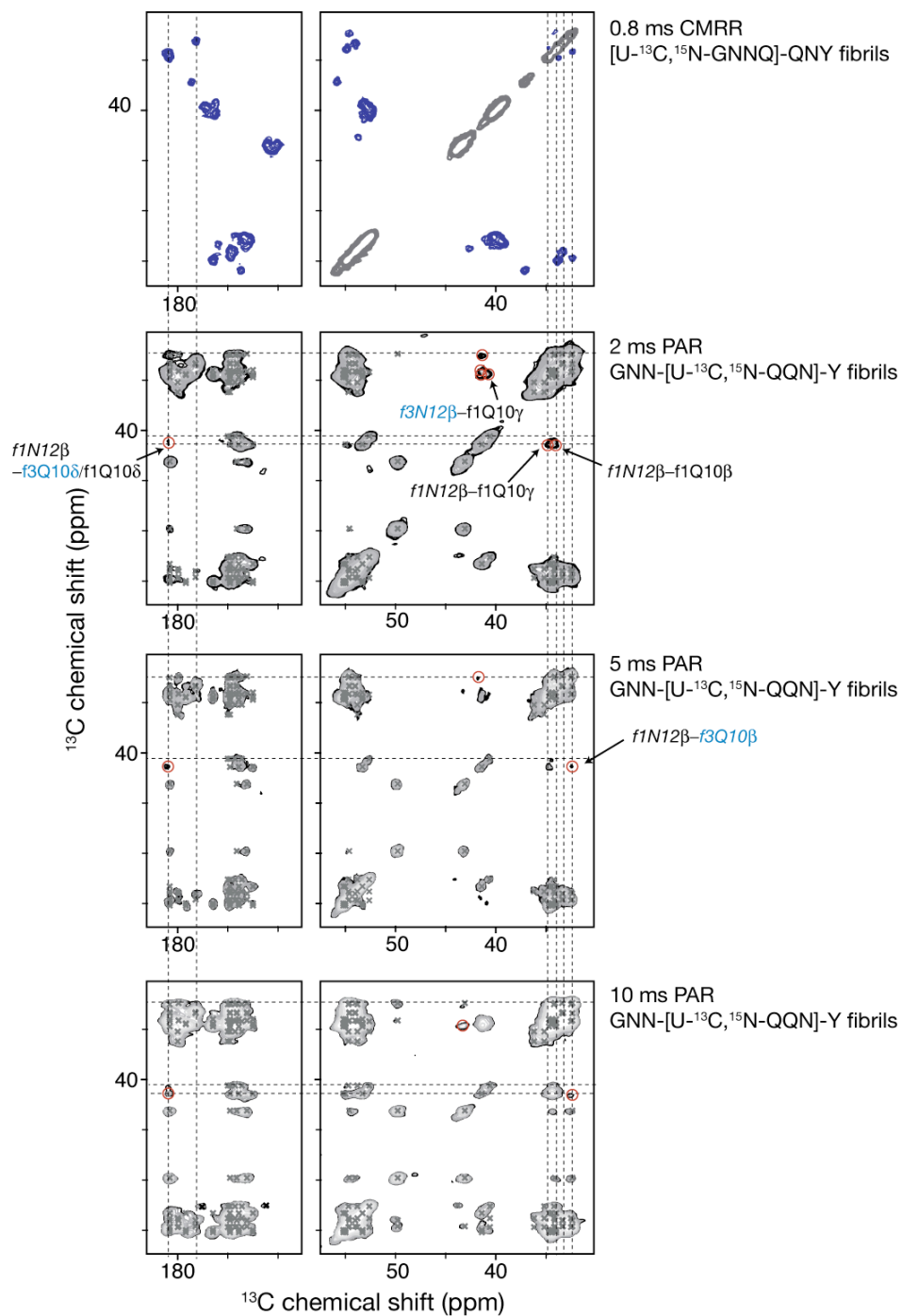


Figure S4. 2D ^{13}C - ^{13}C 0.8 ms CMRR on $[\text{U-}^{13}\text{C}, ^{15}\text{N-GNNQ}]\text{-QNY}$ and variable-mixing-time PAR on $\text{GNN-}[\text{U-}^{13}\text{C}, ^{15}\text{N-QQN}]\text{-Y}$. CMRR was obtained at $\omega_{0\text{H}}/2\pi = 900$ MHz and $\omega_r/2\pi = 20$ kHz. PAR was obtained at $\omega_r/2\pi = 11.3$ kHz and $\omega_{\text{H}0}/2\pi = 700$ MHz. Comparison of the CMRR spectrum, which contains only directly bonded contacts, to the PAR spectra aids the assignment and identification of longer distance and intermolecular cross peaks in the latter.

Table S3. Observed intermolecular contacts supporting various packing interfaces. Shortcut notation for the samples: Q/N mix = 50%-50% GN-[U-¹³C,¹⁵N-N]-QQNY/GNN-[U-¹³C,¹⁵N-Q]-QNY mixture, GNNQ = [U-¹³C,¹⁵N-GNNQ]-QNY, QQN = GNN-[U-¹³C,¹⁵N-QQN]-Y.

Assignment	Ambiguity	Supported interface	Spectrum	Notes
f1-f1				
f1N8C α -f1Q10C β	ambiguous-ambiguous	f1?F-f1EF	PAR on GNNQ	
f1N8C α -f1Q10C γ	ambiguous-unambiguous	f1?F-f1EF	PAR on GNNQ	
f1N9C α -f1Q10C β	unambiguous-ambiguous	f1?F-f1EF	PAR on Q/N mix	
f1N9C'-f1Q10C β	unambiguous-ambiguous	f1?F-f1EF	PAR on Q/N mix	
f1N8C-f1Q10C γ	unambiguous-unambiguous	f1?F-f1EF	PAR on GNNQ	
f1N8C'-f1Q10C β	unambiguous-ambiguous	f1?F-f1EF	PAR on GNNQ	
f1-f3				
f3Q10C'-f1Q10C γ	ambiguous-unambiguous	f3?F-f1EF	PAR on Q/N mix	
f3N12C β -f1Q10C β /C γ	unambiguous-ambiguous	f3EF-f1EF	PAR on QQN	
f1N12C β -f3Q10C β	unambiguous-unambiguous	f1EF-f3EF	PAR on QQN	short distance, present already in 2 ms PAR
f1N12C β -f3Q10C γ	unambiguous-unambiguous	f1EF-f3EF	PAR on QQN	short distance, present already in 2 ms PAR
f3Q10C δ -f1N12C β	ambiguous-unambiguous	f3EF-f1EF	PAR on QQN	short distance, present already in 2 ms PAR
f1-f2				
f1N9C β -f2Q10C β /C γ	unambiguous-unambiguous	f1OF-f2EF	PAR on Q/N mix	
f1N9C β -f2Q10C α	ambiguous-unambiguous	f1OF-f2?F	PAR on Q/N mix	
f1N9C α -f2Q10C β /C γ	unambiguous-unambiguous	f1?F-f2EF	PAR on Q/N mix	
f1Q10C α -f2Q10C β /C γ	ambiguous-unambiguous	f1?F-f2EF	PAR on Q/N mix	
f2Q10C'-f1N9C β	ambiguous-unambiguous	f2?F-f1OF	PAR on Q/N mix	

f1N9C'-f2Q10Cβ/Cγ	unambiguous-unambiguous	f1?F-f2EF	PAR on Q/N mix	
f1N9Cγ-f2Q10Cβ/Cγ	ambiguous-unambiguous	f1OF-f2EF	PAR on Q/N mix	
f1N9Cα-f2Q10Cα	unambiguous-unambiguous	f1?F-f2?F	PAR on Q/N mix	
f1N9Cβ-f2Q10Cβ/Cγ	ambiguous-unambiguous	f1OF-f2EF	PAR on GNNQ	
f2Q10Cα-f1N9Cβ	ambiguous-ambiguous	f2?F-f1OF	PAR on GNNQ	
f2Q10Cδ-f1N9Cα	unambiguous-ambiguous	f2EF-f1?F	PAR on GNNQ/Q/N mix	
f2Q10Cδ-f1N9C'	unambiguous-ambiguous	f2EF-f1?F	PAR on GNNQ/Q/N mix	asymmetric
f1N9N/f1Q10N-f2Q10Cβ/Cγ	ambiguous-ambiguous	f1?F-f2EF	PAIN-CP on GNNQ	
f1Q11Cβ/Cγ-f2Q10Cβ/Cγ	ambiguous-unambiguous	f1OF-f2EF	PAR on QQN	
f2Q10Cδ-f1Q11Cβ/Cγ	unambiguous-ambiguous	f2EF-f1OF	PAR on QQN	
f1Q11Cδ-f2Q10C'	unambiguous-unambiguous	f1OF-f2?F	PAR on QQN	
parallel β-sheet				
f3N9C'-f3Q10Cα	ambiguous-ambiguous	parallel β-sheet	PAR on QN mix	
f1N9Cα-f1Q10Cα	unambiguous-unambiguous	parallel β-sheet	PAR on QN mix	
f2N9Cα-f2Q10Cα	unambiguous-unambiguous	parallel β-sheet	PAR on QN mix	
f3N9Cα-f3Q10Cα	unambiguous-unambiguous	parallel β-sheet	PAR on QN mix	

B-factors for monoclinic and orthorhombic crystals

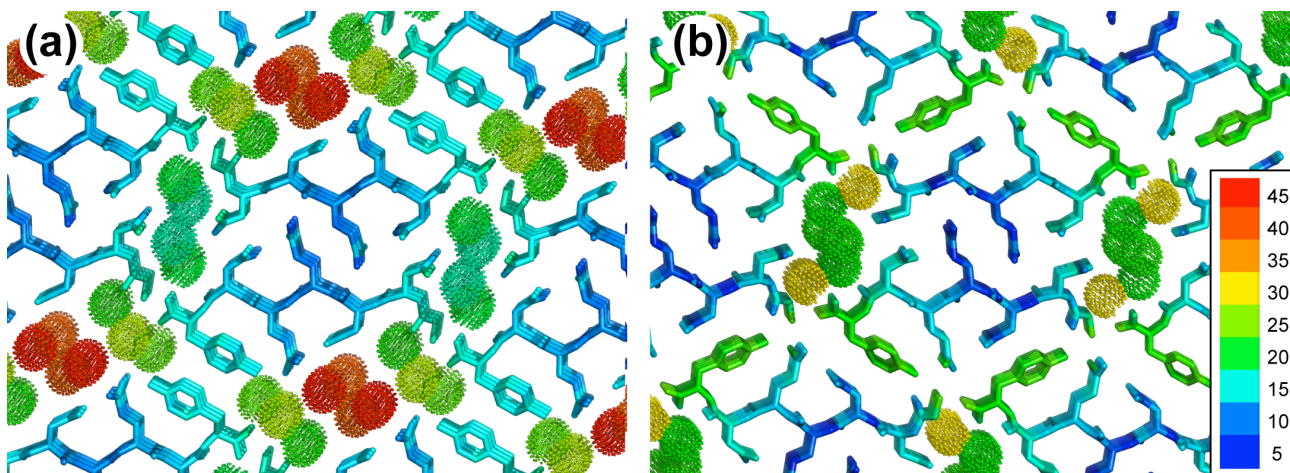


Figure S5. Structure and dynamics of monoclinic (a) and orthorhombic (b) crystal lattices of GNNQQNY at 100K^{3,4}. Both panels employ the same color scale indicating the crystallographic B-factors, as indicated in panel (b). Dotted spheres represent the location and B-factors of crystallographic, but relatively mobile water molecules. Note the significantly increased motion in the orthorhombic crystal form seemingly correlated to the difference in arrangement of the Tyr rings (which have inter-sheet π - π stacking interactions in (a)), consistent with our earlier ssNMR observations.⁵ This figure was prepared with the Pymol program⁶.

References cited in the SI

- (1) Giraud, N.; Bockmann, A.; Lesage, A.; Penin, F.; Blackledge, M.; Emsley, L. *Journal of the American Chemical Society* **2004**, *126*, 11422-11423.
- (2) Torchia, D. A.; Szabo, A. *Journal of Magnetic Resonance* **1982**, *49*, 107-121.
- (3) Nelson, R.; Sawaya, M. R.; Balbirnie, M.; Madsen, A. O.; Riek, C.; Grothe, R.; Eisenberg, D. *Nature* **2005**, *435*, 773-778.
- (4) Sawaya, M. R.; Sambashivan, S.; Nelson, R.; Ivanova, M. I.; Sievers, S. A.; Apostol, M. I.; Thompson, M. J.; Balbirnie, M.; Wiltzius, J. J. W.; McFarlane, H. T.; Madsen, A. O.; Riek, C.; Eisenberg, D. *Nature* **2007**, *447*, 453-457.
- (5) van der Wel, P. C. A.; Lewandowski, J. R.; Griffin, R. G. *Biochemistry*. in press.
- (6) DeLano, W. L.; DeLano Scientific: San Carlos, CA, USA, 2002.
- (7) Berryman, J. T.; Radford, S. E.; Harris, S. A. *Biophysical Journal* **2009**, *97*, 1-11.
- (8) Esposito, L.; Paladino, A.; Pedone, C.; Vitagliano, L. *Biophys. J.* **2008**, *94*, 4031-4040.
- (9) Esposito, L.; Pedone, C.; Vitagliano, L. *Proceedings of the National Academy of Sciences* **2006**, *103*, 11533-11538.
- (10) Park, J.; Kahng, B.; Hwang, W. *PLoS Comput Biol* **2009**, *5*, e1000492.
- (11) Meli, M.; Morra, G.; Colombo, G. *Biophys. J.* **2008**, *94*, 4414-4426.